UNIVERSITY OF TWENTE

MASTER THESIS

Sorting catalytic particles in microfluidics using the Magnus effect

---

Author:
Hans KEIZER

Supervisor:
dr.ir. W. OLTHUIS
M. SOLSONA, Msc.
Prof.dr.ir. L. ABELMANN

A thesis submitted in fulfillment of the requirements for the degree of Master of Science

in the

BIOS Group
University of Twente

August 17, 2018

UNIVERSITY OF TWENTE

Abstract

Faculty of Electrical Engineering,
Mathematics & Computer Science
University of Twente

Master of Science

Sorting catalytic particles in microfluidics using the Magnus effect

by Hans KEIZER

Fluid catalyic cracking (FCC) particles are currently used in almost half of the gasoline production to crack hydrocarbons into fuels. However, during the FCC process the particles get deactivated due to accumulation of some metals like Iron (Fe), Nickel (Ni) and Vanadium (V). To investigate the activity of FCC particles for different Fe loadings, the particles were sorted using magnetophoresis. This analysis showed that the activity of a particle decrease for a higher Fe loading. However, it was observed that not all particles with a high Fe loading were inactive. Based on this observation, two different distributions of Fe are likely, namely an uniform distribution or cluster forming. Therefore a sorting mechanism to sort the FCC particles based on their Fe distribution is needed to investigate the activity of the particles even better. The sorting of the particles was done in microfluidics using the Magnus effect. This effect is expressed by rotating particles placed in an external rotating field. Particles with clusters will experience a torque and start to rotate, whereas particles with an uniform distribution will not rotate. The microfluidic chip is designed to focus the particles solely using the gravitational force. Furthermore, the particles move through the chip without interacting with the walls of the system. The model created to predict the magnetic field, rotational length, gravitational force, magnetic force, torque, Magnus force to obtain the particle trajectories, is validated experimentally using Janus Particles. The ability to sort particles based on the Magnus effect has been shown using both Janus and FCC particles. The measured deflection was between 25 and 65 μm, which is too small to sort the particles using this chip. However, if the starting position of the particles and the deflection due to the Magnus effect is improved, the particles can potentially be sorted using the Magnus effect.

Acknowledgements

I would like to thank many different people for their help during my research. First of all, I would like to thank the members of the committee, Wouter Olthuis, Leon Abelmann and Miguel Solsona. During many usefull meetings, Wouter helped me to stay focused on the end goal and kept me on the right track. Furthermore, I owe many thanks to the every enthusiastic Leon for his help to understand all the different forces acting upon a particle in such a simple system. Sometimes you blow me away with just one simple question, but this only motivated me to work harder and to be able to answer all your future questions! It was a real pleasure to work with you during my internship and now during my master thesis. Hopefully the new designed OD meter works properly. The last member of the comittee I would like to thank is Miguel. I did my bachelor assignment with you and this left such a great experiences, that I was very happy to be asked to do my master assignment with you. Many, many thanks for all the help and motivation during this rollercoaster of a master assignment. I am really happy with the final result, which is achieved for a great part due to your help! The sentence: "Litlle by little", I won't forget easily. Besides the serious stuff, I learned a lot from your great pool of wisdom. Besides the committee I would like to thank several other people at BIOS. First of all I need to thank Gerrit for standing by me for the last year. It had a real great time together with you during my internal internship and my master thesis. After one complete year of my madness, you are finally free! I wish you all the best in the coming years and you are always welcome to have a little beer. Further I would like to thank Jordi for the useful discussions and proof reading of my thesis. Another person, which helped me a lot, is my mental coach Eiko. This guy knows how to trigger me and let me rise to new heights, so thanks a lot. Furthermore, many thanks go out to LdH and BdB for all the laughs and usefull tips and tricks I learned. Lastly I want to thank all the other people at BIOS. I really enjoyed my time here and met a lot of amazing people. One of my highlights was the batavieren race as Jackqueoline together with TinTin. Straight forever!

Contents

List of Abbreviations

FCC	**F**luid **C**racking **C**atalityc
Fe	Iron
Ni	**N**ickel
V	**V**anadium
Re	**Re**ynolds number

Chapter 1

Introduction

Currently fluid catalytic cracking (FCC) particles are used in almost half of the gasoline production. These particles are used for cracking long-chain hydrocarbons into gasoline and base chemicals [1, 2, 3]. During the FCC process, the particles get deactivated due to accumulation of metals like Iron (Fe), Nickel (Ni) and Vanadium (V). These metals accumulate mostly on the surface of the particles, which prevents the hydrocarbons to reach the pores of the FCC particles [2]. To maintain a high efficiency, a fraction of the used particles is replaced by fresh ones each day. This fraction of used particles is chosen randomly and not based on metal loading or activity. To investigate the activity of particles based on metal loading, two methods are known in literature. The first method is sorting the particles based on their difference in densities due to different metal loadings of each particle [2]. The second method is using magnetophoresis, which is based on the difference in magnetic properties due to the different metal loadings [1]. Solsona et al show a method for sorting the particles in a microfluidic system with a high throughput [1]. This method sorted the particles solely based on their Fe loading and not on their Ni or V loading. After the sorting of the particles, the activity was analyzed. Acidity can be used to indicate how acitive a particle still is. If the acidity decreases, also the activity of the particle decreases [1]. There was a decrease of acidity for an increasing amount of observed Fe, as can be seen in Fig.1.1. However, it was also observed that not all particles with a high Fe loading were inactive.

Based on this observation, two different distributions of Fe are expeted, namely a homogeneous distribution or a distribution with clusters of Fe. These two distributions can be seen in Fig.1.2.

These clusters of Fe block only a small part of the surface of the particle, while the rest of the particle still can be active. To get a better understanding of the deactivation of the particles, a method to separate the particles based on their Fe distribution is desired.

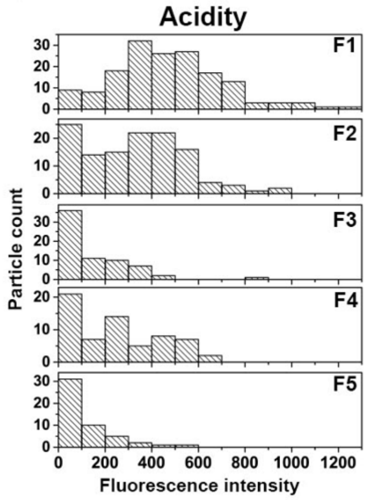

FIG. 1.1: Histograms of the average fluorescence intensity per FCC particle. The amount of Fe increases from F1 to F5, where F1 has almost no Fe [1].

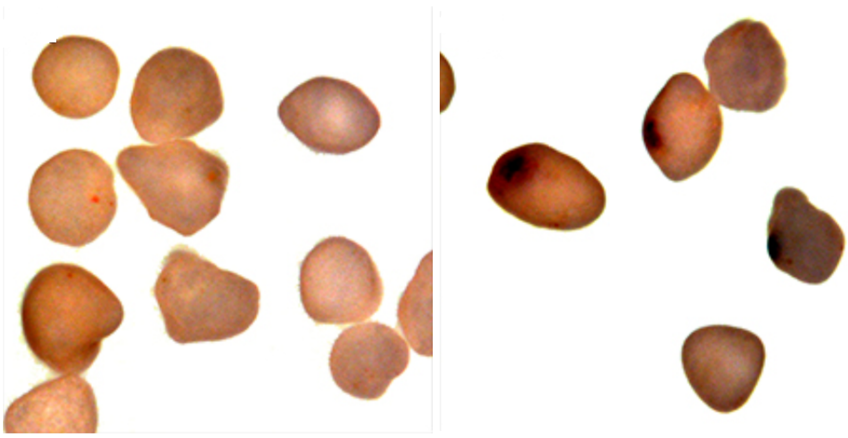

(A) (B)

FIG. 1.2: The two expected distributions of Fe on a particle. On the left the uniform distribution of Fe (A) and on the right the cluster forming (B) [1].

Rem showed that magnetic particles can be separated from a mixture using the Magnus effect [4]. In this work the particls are rotating while moving through the liquid. The rotation of the particles creates a force perpendicular to the movement of the particles and due to this sideway force the particles can be separated from the liquid [4]. This separation method can be applied to the FCC particles. Upon application of a rotating magnetic field, some particles will rotate due their Fe distribution while others will not. The particles with clusters will try to align their magnetic moment with the external magnetic field. Due to the difference in direction of the field and the moment a torque is created. However, for particles with a homogeneous distribution it is more favorable to align their moment within their magnetic layer than to rotate the whole particle. Based on this difference, the particles with different distributions will have different behaviors and can therefore be sorted. To be able to control the small FCC particles with a diameter between 50 - 150 μm [3], a microfluidic device will be used. Microfluidic devices are highly advantageous since they allow for single particle analysis, offer (spatial and temporal) control of the relevant parameters [5,6] and inertia is neglible at this scale [5, 6].

The goal of this research is to sort FCC particles based on their Fe distribution using the Magnus effect in a microfluidic system. Janus particles will be used to give a proof of principle. These Janus particles have a magnetic layer on half of the particle. To obtain particles with similiar properties, these particles will be sorted using magnetophoresis. Furthermore, Janus particles with diameters in the same range as FCC particles will be used.

This report starts with theory about microfluidic systems, magnetic forces and the Magnus effect in Chapter 2. This theory will be used to design the microfluidic system and to choose a magnet in Chapter 3. In Chapter 4, the used materials and the measurement setup and protocol will be described. The results will be discussed in Chapter 5. The final chapter, Chapter 6, will conclude with the conclusions and will give recommendations for the future.

Chapter 2

Theory

In this chapter the background theory will be discussed. First the microfluidic forces and the Reynolds number will be treated. Next the magnetic field and its forces will be explained, followed by some theory about the torque acting on a particle. Finally, the Magnus effect will be discussed. If all the forces are discussed, the model for the trajectory of a particle will be explained. This theory will be the basis for the design of the system.

2.1 Microfluidics

The microfluidic device will be operated in a vertical direction under static conditions, which means no flow of liquid and no external pressure is applied. In this way, the situation is as simple as possible, as there are no fluid dynamics present. The particles will move through the liquid due to the gravitational force. However, the fluid gives a counter force, known as the drag force. The situation can be seen in Fig.2.1.

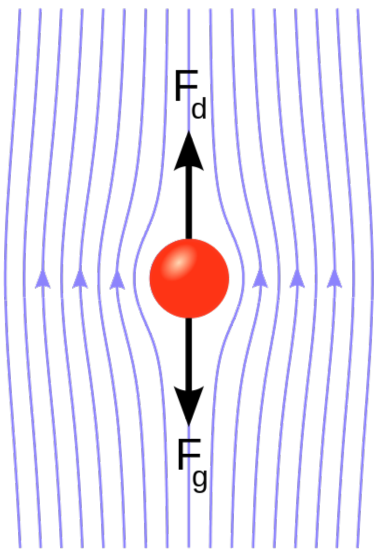

FIG. 2.1: A particle moving through a liquid due to the gravitational force (F_g). The opposing force is the drag force (F_d) created by the liquid [7].

These two forces were described by Stokes' law. For the description of these two forces the following assumptions were made [8]:

- The flow surrounding the particle is laminar
- The particles are spherical
- The material properties are homogeneously distributed throughout the material
- The particles surface is smooth
- No interaction between individual particles

The flow surrounding the particle is often determined by the particle Reynolds number (Re_p). This parameter is explained in Sec.2.1.

Gravitational force

As mentioned before, no flow or external pressure will be applied. The main force exerted on the particles will be the gravitational force which can be mathematically described by the Stoke's law [8]:

$$F_\mathrm{g} = \frac{4}{3}(\rho_\mathrm{p} - \rho_\mathrm{f}) g \pi r_\mathrm{p}^3, \tag{2.1}$$

where g is the gravitational acceleration [$\mathrm{m\,s^{-2}}$], ρ_f and ρ_p are the densities of the fluid and particles respectively [$\mathrm{kg\,m^{-3}}$] and r_p is the radius of the spherical particle [m].

From Eq.2.1 several things can be concluded. The first thing to notice is the direction of the force. If the particle has a higher density than the fluid, the force will be positive and the particle will sink. If the particle has a lower density, the particle will move upwards. Another thing which can be concluded concluded is the resulting force will increase when the difference between the particles and fluid density increases.

Drag force

If a particle is moving with respect to the surrounding liquid it experiences a opposing force. This opposing force is called the translational drag force (F_D). For a sphere moving through the liquid with a constant velocity u_p, the force can be described using Stokes' law:

$$F_\mathrm{D} = 6\pi\eta r_\mathrm{p} u_\mathrm{r}, \tag{2.2}$$

where η is the viscosity of the fluid [Pa s] and u_r is the relative velocity between the fluid and the particle [$\mathrm{m\,s^{-1}}$]. In this situation is u_r equal to u_p, because there is no flow of liquid.

For rotational movement instead of translational movement, another drag force is introduced. This rotational drag force (F_{Dr}) depends on the shape of the particle. For a sphere this force can described as follows [9]:

$$F_{\mathrm{Dr}} = 8\pi\eta r_{\mathrm{p}}^{3}\Omega_{\mathrm{r}}, \tag{2.3}$$

where Ω_{r} is the relative rotational velocity between the particle and the fluid.

Reynolds number

An important parameter to determine the fluid behavior in microfluidics is the Reynolds number (Re), or sometimes called the particle Reynolds number (Re_p). This dimensionless quantity is a measure to distinguish between two flow regimes. For low Reynolds numbers (Re < 100) the regime is purely laminar, whereas it is turbulent for high Reynold numbers (Re>2000). The Reynolds number is defined as a ratio between the inertial forces and viscous forces[10]:

$$Re = \frac{\rho_{\mathrm{f}}\, u_{\mathrm{r}}\, L}{\eta}, \tag{2.4}$$

where L is the characteristic length of the channel [m]. Stoke's law assumes a laminar flow and therefore the Reynolds number should be below 100.

2.2 Magnetic force

For the creation of an external magnetic field, two options are available, namely a permanent magnet or an electromagnet. In this research, a permanent bar magnet is chosen as will be further elaborated on in Section 3.2. The magnet will have an magnetization in the z-direction as can be seen in Fig.2.2.

The magnetic field produced by a permanent magnet can be predicted for every direction using an analytical solution: [11]

$$B_x(x,y,z) = \frac{\mu_0 M_s}{4\pi}\sum_{k=1}^{2}\sum_{m=1}^{2}(-1)^{k+m}\ln\left(\frac{(y-y_1)+[(x-x_m)^2+(y-y_1)^2+(z-z_k)^2]^{1/2}}{(y-y_2)+[(x-x_m)^2+(y-y_2)^2+(z-z_k)^2]^{1/2}}\right), \tag{2.5}$$

$$B_y(x,y,z) = \frac{\mu_0 M_s}{4\pi}\sum_{k=1}^{2}\sum_{m=1}^{2}(-1)^{k+m}\ln\left(\frac{(x-x_1)+[(x-x_1)^2+(y-y_m)^2+(z-z_k)^2]^{1/2}}{(x-x_2)+[(x-x_2)^2+(y-y_m)^2+(z-z_k)^2]^{1/2}}\right), \tag{2.6}$$

$$B_z(x,y,z) = \frac{\mu_0 M_s}{4\pi}\sum_{k=1}^{2}\sum_{n=1}^{2}\sum_{m=1}^{2}(-1)^{k+m}\times \tag{2.7}$$
$$\tan^{-1}\left[\frac{(x-x_n)(y-y_m)}{(z-z_k)[(x-x_n)^2+(y-y_m)^2+(z-z_k)^2]^{1/2}}\right].$$

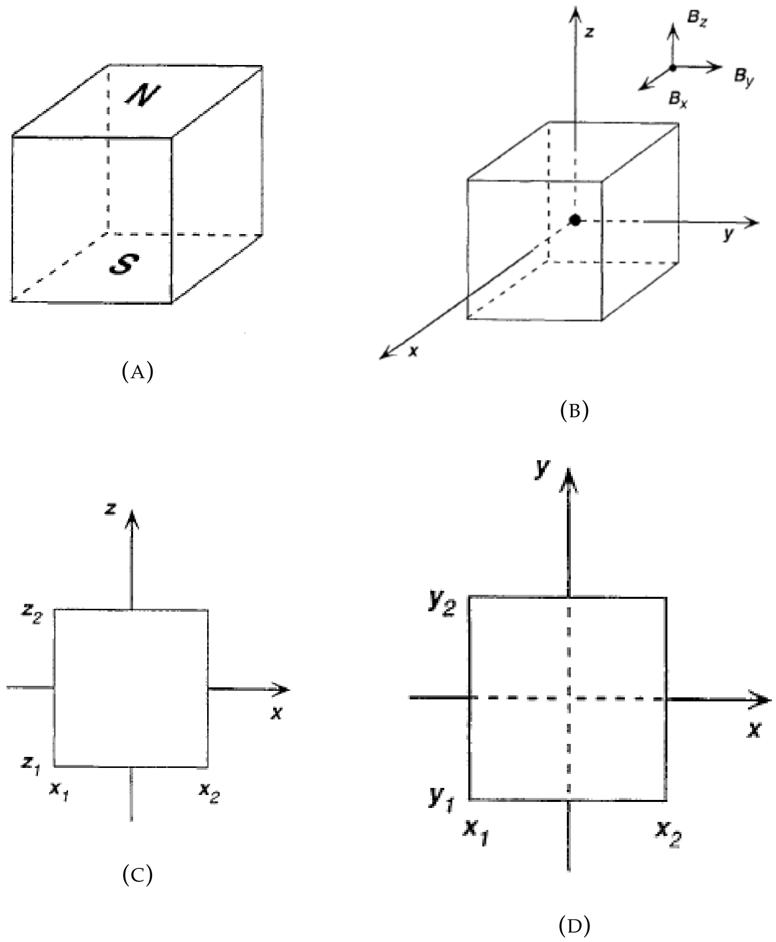

FIG. 2.2: The magnetization of the magnet (A) together with the orientation of the magnet (B). Furthermore the names of edges of the magnet used for the analytical solution (C,D) [11].

where μ_0 is the permeability of free space [H m^{-1}], M_s the magnetization of the magnet [A m^{-1}], x_n, y_m and z_k (n=m=k=1,2) are the coordinates of magnets corners with respect to the fixed coordinate system [m], as shown in Fig.2.2c and Fig.2.2d. From these equations it becomes clear that only a few parameters can be chosen to optimize the magnetic field, namely M_s and the size of the magnet (x_n, y_m and z_k).

If a particle is moving through a magnetic field, it will experience a magnetic force (F_m). This magnetic force can be expressed as [12]

$$F_m = \mu_0 V_{pmag} (M_p \cdot \nabla) H_a, \tag{2.8}$$

where V_{pmag} is the magnetic volume of the particle [m^3], M_p is the magnetization of the particle [A m^{-1}] and H_a is the applied magnetic field intensity[A m^{-1}]. The relation between the calculated magnetic field B and the field intensity H can be described as:

$$H_a = \frac{B}{\mu_0}. \tag{2.9}$$

For the magnetization of the particle a linear model will be used. The magnetization can be described below the saturation value (M_{sp}) as:

$$M_p = \chi_p H_{in}, \tag{2.10}$$

where χ_p is the unitless susceptibility of a particle and H_{in} is the applied field intensity [A m^{-1}]. For H_{in} two different situations can be modeled. The first situation is the particle without an inner demagnitisation field, which results in that $H_{in} = H_a$.

For H_{in} , two different situations can be modeled, namely the particle without and with a demagnitization field. In the first situation, this results in $H_{in} = H_a$. In the second situation however, the field is opposing the external field which results in a decreased applied field. The resulting field in this situation can be described as:

$$H_{in} = H_a - \frac{M_p}{\gamma}, \tag{2.11}$$

where γ is the unitless demagnetisation factor. This demagnetisation factor depends on the shape of the particle and the orientation. In this case, the particles are modeled as spheres. The demagnetisation factor is not orientation dependent for a sphere and γ is $\frac{1}{3}$ for the x, y, z-components.

The resulting magnetic force can be decomposed into different components if the demagnetisation field is not taken into account:

$$F_m(x, y, z) = F_{mx}(x, y, z)\vec{x} + F_{my}(x, y, z)\vec{y} + F_{mz}(x, y, z)\vec{z}, \tag{2.12}$$

where $\vec{x}, \vec{y}$ and $\vec{z}$ are unity vectors. Each component of the magnetic force can be calculated individually [12]:

$$\begin{aligned} F_{mx}(x, y, z) = \mu_0 V_{pmag} \chi_p \Bigg[& H_{ax}(x, y, z)\frac{\delta H_{ax}(x, y, z)}{\delta x} + H_{ay}(x, y, z)\frac{\delta H_{ax}(x, y, z)}{\delta y} + \\ & H_{az}(x, y, z)\frac{\delta H_{ax}(x, y, z)}{\delta z} \Bigg], \end{aligned} \tag{2.13}$$

$$\begin{aligned} F_{my}(x, y, z) = \mu_0 V_{pmag} \chi_p \Bigg[& H_{ax}(x, y, z)\frac{\delta H_{ay}(x, y, z)}{\delta x} + H_{ay}(x, y, z)\frac{\delta H_{ay}(x, y, z)}{\delta y} + \\ & H_{az}(x, y, z)\frac{\delta H_{ay}(x, y, z)}{\delta z} \Bigg], \end{aligned} \tag{2.14}$$

$$F_{mz}(x,y,z) = \mu_0 V_{pmag} \chi_p \left[H_{ax}(x,y,z) \frac{\delta H_{az}(x,y,z)}{\delta x} + H_{ay}(x,y,z) \frac{\delta H_{az}(x,y,z)}{\delta y} + \right. \\ \left. H_{az}(x,y,z) \frac{\delta H_{az}(x,y,z)}{\delta z} \right]. \tag{2.15}$$

From these equations it can be concluded that the magnetic force a particle experiences, is depending on a variety of variables. It depends on the magnetization and magnetic volume of the particle itself, but also on the strength and gradient of the magnetic field intensity H_a.

2.3 Torque

If a magnetic particle is placed inside a magnetic field and the particles magnetic moment and the field are not aligned, a torque (Γ) is created. This phenomena is illustrated in Fig.2.3.

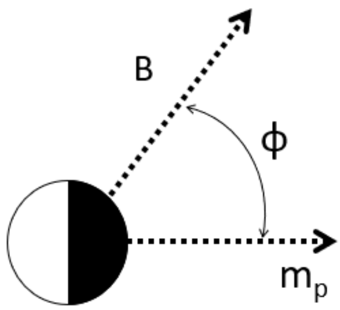

FIG. 2.3: A particle experiences a torque due to the difference in the direction of its magnetic moment (m_p) and the direction of the magnetic field (B). This difference is characterized by the angle ϕ.

The total torque created by the external field can be described as follows [13]:

$$\Gamma = B \times m_p = m_p B \sin(\phi). \tag{2.16}$$

If the particles moment is not fully saturated, this equation can be rewritten to:

$$\Gamma = \chi_p B^2 \sin(\phi), \tag{2.17}$$

where ϕ is the angle between the direction of the magnetic field and the moment of the particle and χ_p is the susceptibility of the particle [Am^2/T]. Notice χ_p is not unitless in specific situation. This is due to the fact that it relates different magnetic properties, which are m_p and B in this case.

The applied torque is maximal for an angle of 90° and becomes smaller for lower angles. Because the magnetic moment of a particle cannot be changed, the only way to increase the torque is to increase the strength of the magnetic field.

2.4 Magnetic moment of a particle

The magnetic moment of a magnetic particle (m_p) depends on several factors related to the material, namely the magnetic properties and the amount of material. This material will have a certain magnetization (M_p). The total moment created by the magnetization of such a particle can be calculated as follows:

$$m_p = M_{sp} V_{pmag}, \tag{2.18}$$

where M_{sp} is the magnetization of a particle [$\mathrm{A\,m^{-1}}$], V_{pmag} is the volume of the magnetic material [$\mathrm{m^3}$] and m_p the magnetic moment of a particle [$\mathrm{A\,m^2}$]. To calculate the thickness of the magnetic layer on the Janus particles from the volume of magnetic material, another step is needed. The layer is applied on half of the surface of a sphere with a radius of 50 µm. The thickness of the layer can be calculated as follows:

$$r_{pmag} = \sqrt[3]{\frac{3}{2\pi}(V_{pmag} - r_p^3)}. \tag{2.19}$$

2.5 Magnus effect

The Magnus force is associated with spinning objects moving through air or a fluid. A lot of ball sport players like soccer, tennis or baseball players make use of it. But what causes this force and what is the effect of this force? The Magnus force is a force acting upon a spinning object moving through air or a liquid. It creates a lift on the object perpendicular to the movement of the object [14]. There are two different explanations for this lift force. The first explanation is often used in macro scale. For this macro scale holds that the Reynolds number is several magnitudes higher than for micro scale. For the marco scale, the Reynolds number is often higher than 3000, while for micro scale it is below 10. The first explanation will be given with the use of a rotating tennis ball. If the ball is moving through the air while it is rotating, it will accelerate the surrounding air at one side of the ball, while it slows down the air at the other side. This situation can be seen in Fig.2.4, where the ball moves to the right. There is an imbalance between the pressure at the top and bottom of the ball created. This imbalance will create an downward force, which is known as the Magnus force [14].

This explanation has its downside. For low Reynolds numbers, which are usually present inside a microfluidic system, the explanation is not applicable. If the Reynolds number is a lot smaller than 1, the assumption can be made that there is Stokes flow [8]. This assumption is made due to the sizes of a microfluidic chip and

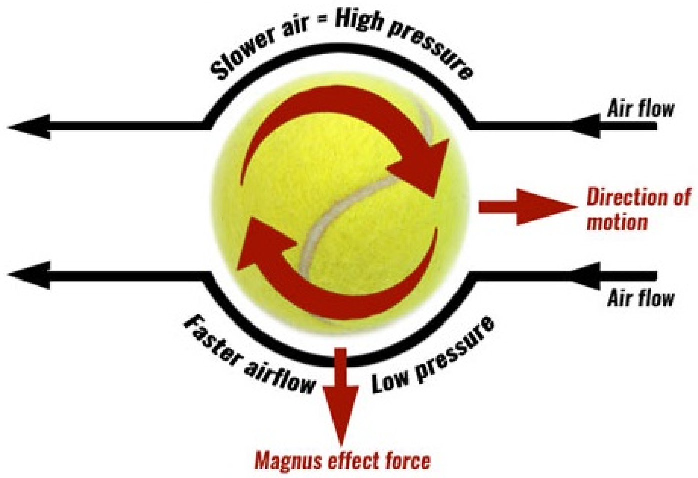

FIG. 2.4: The situation for a rotating tennis ball moving to the right. The rotation of the ball makes the air move slower on the top of the ball, while it acceralates the air at the bottom. This will create a high pressure at the top of the ball, while it will create a low pressure at the bottom. This pressure difference will cause a downwards force [15].

therefore the expectation is that the Reynolds number will be smaller than 1. For a Stokes flow of an incompressible fluid (Re=0), there is no pressure difference across the width or height of the channel. The only pressure difference is along the channel and is created due to external pressures [16]. There the second explanation comes into play. When the particle does not rotate, the flow of the liquid passing the particle is not deflected as can be seen in Fig.2.5a. However when the particle is rotating to the right, the fluid is deflected downwards. This situation can be seen in Fig.2.5b. The liquid passing at the top of the particle will be dragged down due to the contact with the surface of the rotating particle. At the bottom of the particle the liquid is slowed down, but not deflected. Therefore there is a net amount of liquid going down, which will have a force downwards. According to Newton's third law there will be an opposing force acting upon the particle upwards. This opposing force is called the Magnus force and is described by Heinrich Gustav Magnus. The force can be written in an equation as follows [17]:

$$F_{Magnus} = \pi \rho_f r_p^3 \Omega \times u_r. \tag{2.20}$$

As becomes clear from the cross product the Magnus effect is biggest when the rotation of the particle is perpendicular to the movement direction. From this equation, it seems that the relative downward velocity should be as high as possible. However, if the velocity is higher, the time where the Magnus effect acts upon the particle will be smaller. Therefore an higher relative velocity downwards does not have to be the solution for a high deflection.

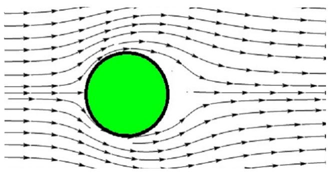

(A)

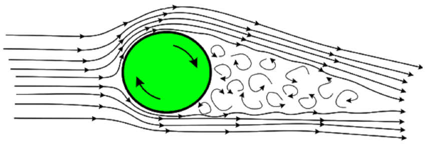

(B)

FIG. 2.5: The fluid lines passing by a particle for a non rotating particle (A) and a rotating particle (B).

2.6 Model description

To get an impression on how a particle behaves, a force model will be made. The goal of this model is to obtain the trajectory of a particle moving through the channel of the chip. This trajectory will consist of components in the x, y and z direction. The assumption is made that the particle will not have any interaction with the walls of the system. It is important to know how the magnet will be placed compared to the system. The magnet will have its magnetization along the z-direction and will be placed at a distance d in the y-direction. As mentioned before, the driving force of the system will be gravity (F_g) which will be opposed by a drag force (F_{Dz}). The magnetic force in the z direction (F_{mz}) will be neglected, because it will be a lot smaller than the gravity force. All these forces are acting along the z-direction of the system. These situation can be seen in Fig.2.6a. This two forces will create an equilibrium and from this, the equilibrium velocity of the particle can be calculated.

$$F_g = F_{Dz}, \tag{2.21}$$

$$(\rho_\mathrm{p} - \rho_\mathrm{f}) g \pi r_\mathrm{p}^3 \frac{4}{3} = 6\pi\eta r_\mathrm{p} u_\mathrm{r}, \tag{2.22}$$

$$u_\mathrm{rz} = \frac{2}{9}\frac{(\rho_\mathrm{p} - \rho_\mathrm{f})\, g\, r_\mathrm{p}^2}{\eta}. \tag{2.23}$$

For the y-direction, the attraction to the magnet is dominating. The attraction is created by the magnetic force (F_{my}). Also in this situation the particle will feel an opposing drag force (F_{Dy}), which can be seen in Fig.2.6b. The equilibrium these two forces create will also result in a velocity. This velocity will be in the y-direction

$$F_{my} = F_{Dy}. \tag{2.24}$$

For the simplicity the magnetic force will not be written completely, because it is a long equation and will not help to understand the situation better.

$$u_\mathrm{ry} = \frac{F_{my}}{6\pi\eta r_\mathrm{p}}. \tag{2.25}$$

For the x-direction, several forces play a role. First there is the magnetic force (F_{mx}), second the Magnus force (F_{magnus}) and last the drag force (F_{Dx}). These forces

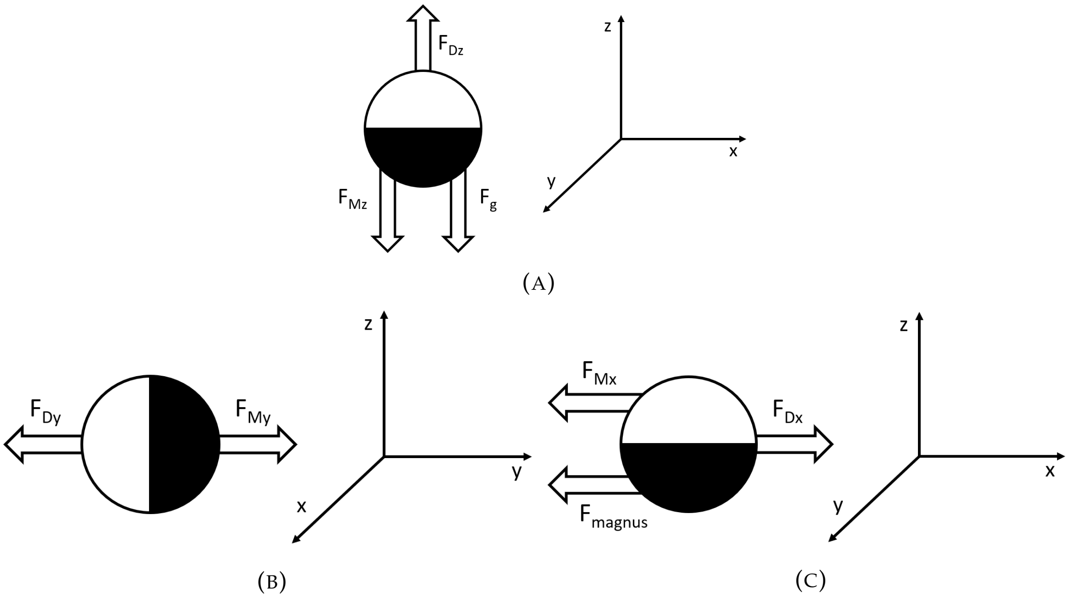

FIG. 2.6: The forces acting upon a particle for each direction. In the z-direction the gravity force and the opposing drag force are present (A). For x-direction the magnetic force together with the Magnus force are opposed by the drag force (B). For the y-direction only the magnetic force is acting upon the particle together with the drag force (C).

can interact differently and this creates three different possible scenarios:

1. The particles doesn't rotate and there is no Magnus force acting upon the particle. The particle deflects due to the magnetic force (F_{mx}).

2. The particle rotate and there is a Magnus force acting upon the particle. The magnetic force and the Magnus force have the same direction.

3. The particle rotate and there is a Magnus force acting upon the particle. The magnetic force and the Magnus force have opposite direction.

In all these scenarios, the drag force (F_{Dx}) will oppose the force or sum of forces.

For the first scenario only the magnetic force and drag force are present. The force equilibrium for this scenario becomes:

$$F_{mx} = F_{Dx}. \tag{2.26}$$

This is the same situation as in the y-direction and the final velocity becomes:

$$u_{\mathrm{rx}} = \frac{F_{mx}}{6\pi\eta r_{\mathrm{p}}}. \tag{2.27}$$

The second scenario can be described by the equilibrium of forces and is illustrated in Fig.2.6c:

$$F_{mx} + F_{magnus} = F_{Dx}. \tag{2.28}$$

Again the magnetic force will not be written fully due to the complexity of the equation.

$$F_{myx} + \pi r_{\mathrm{p}}^3 \rho_f \Omega u_{ry} = 6\pi\eta r_{\mathrm{p}} u_{\mathrm{rx}}. \tag{2.29}$$

The resulting equilibrium velocity can be calculated by rewriting this equation:

$$u_{\mathrm{rx}} = \frac{F_{myx} + \pi r_{\mathrm{p}}^3 \rho_f \Omega u_{ry}}{6\pi\eta r_{\mathrm{p}}}, \tag{2.30}$$

$$u_{\mathrm{rx}} = \frac{F_{myx}}{6\pi\eta r_{\mathrm{p}}} + \frac{1}{6}\frac{r_{\mathrm{p}}^2 \rho_f \, \Omega \, u_{ry}}{\eta}. \tag{2.31}$$

For the third scenario, the assumption is made that the Magnus force is bigger than the magnetic force. The force equilibrium becomes:

$$F_{magnus} - F_{mx} = F_{Dx}. \tag{2.32}$$

Again the magnetic force will not be written fully due to the complexity of the equation.

$$\pi r_{\mathrm{p}}^3 \rho_f \Omega u_{ry} - F_{mx} = 6\pi\eta r_{\mathrm{p}} u_{\mathrm{rx}}. \tag{2.33}$$

The resulting equilibrium velocity can be calculated by rewriting this equation:

$$u_{\mathrm{rx}} = \frac{\pi r_{\mathrm{p}}^3 \rho_f \Omega u_{ry} - F_{mx}}{6\pi\eta r_{\mathrm{p}}}, \tag{2.34}$$

$$u_{\mathrm{rx}} = \frac{1}{6}\frac{r_{\mathrm{p}}^2 \rho_f \, \Omega \, u_{ry}}{\eta} - \frac{F_{mx}}{6\pi\eta r_{\mathrm{p}}}. \tag{2.35}$$

Now that all the velocities in all directions are known, the covered distances in each direction can be calculated.

For the rotation of the particles two forces are important, namely the rotational drag force (F_{Dr}) and the external applied torque (Γ). This situation can be seen in Fig.2.7. This force equilibrium determines the maximum rotational velocity of a particle.

$$\Gamma = F_{Dr}, \tag{2.36}$$

$$\chi_p B^2 = 8\pi\eta r_{\mathrm{p}}^3 \Omega_{\mathrm{r}}, \tag{2.37}$$

$$\Omega_{\mathrm{r}} = \frac{\chi_p B^2}{8\pi\eta r_{\mathrm{p}}^3}. \tag{2.38}$$

Another way to look at this equation is to look at the needed magnetic field strength to rotate the particle with a certain strength. This minimum strength B_{min}

can be calculated as follows:

$$B_{min} = \sqrt{\frac{8\pi\eta r_\mathrm{p}^3\Omega_\mathrm{r}}{\chi_p}}. \tag{2.39}$$

The magnetic field will have a different strength at different places in the channel. If the strength at each place of the particle trajectory is determined, the length of rotation can be calculated.

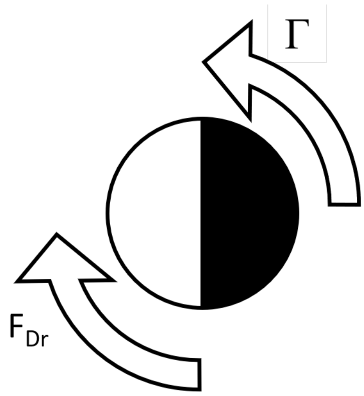

FIG. 2.7: The external torque acting upon the particle is counteracted by the rotational drag from the liquid.

Chapter 3

Design

In this chapter the design of several aspects of the system will be discussed. First, it will start with the design of the microfluidic chip used during the experiment. Second, the choice of magnet will be treated. Finally, the fluid for the experiments will be chosen.

3.1 Microfluidic chip

For the chip design, several aspects have to be taken into account. 1) All particles should have identical starting positions, 2) the main channel should be big enough for the particles to deflect from their starting position without interacting with the channel walls and 3) the particles should be clearly visible for trajectory tracking. The final chip design is illustrated in Fig.3.1.

To ensure identical particle starting positions, the particles have to be focused inside the channel. Since no external pressure or flow is present, state of the art flow-focusing methods are not suitable. Therefore, another focussing method is designed, which exploit the gravitational force. The particle inlet, which is designed to focus the particles into the channel, can be seen in Fig.3.2a. The inlet is positioned at the top part of the chip and consists of three cylinders under and angle of three degrees compared to the z-axis, of which the middle cylinder has an opposing direction compared to the other two. Particle focusing is achieved by letting the particles roll over the bottom of the cylinders. Due to particle-wall and particle-particle interaction as well as gravity the particles will roll through the cylinders one by one. By using three cylinders instead of one, the amount of focused particles is increased. Due to gravity, the particles flow through the cylinders and have a narrow velocity distribution. Small differences in particle velocity are expected to be caused by variances in particle density. As a result of the narrow velocity distribution, a stable starting position is created when they exit the inlet cylinder into the channel.

In addition to the particle inlets, two inlets are added to make it possible to get rid of debris inside the system and prepare the system for a measurement. They can be used to let the fluid in or let the air from inside the chip out. Since the placement of the three individual inlets can influence the system, the position of the inlets is chosen with some care. The final inlet positions are shown in Fig.3.2b. The two fluid inlets are positioned in the two corners of the channel to prevent influence of one inlet on another. Subsequently, the particle inlet is placed at the other side (y-axis) of the channel for two main reasons. First, to minimize the influence of the fluid inlets and second, to decrease the attraction towards the magnet compared to a position above the middle of the channel. This smaller attraction towards the magnet gives us the ability to bring the magnet closer whilst still preventing the particles from touching the wall. As can be seen in Fig.3.2a, the inlet is not completely above the center of the channel. This placement is chosen based on the experience that the particle will not fall straight out of the inlet, but slightly towards the right (x-axis) due to some adhesion forces at the transition between the cylinder and the channel.

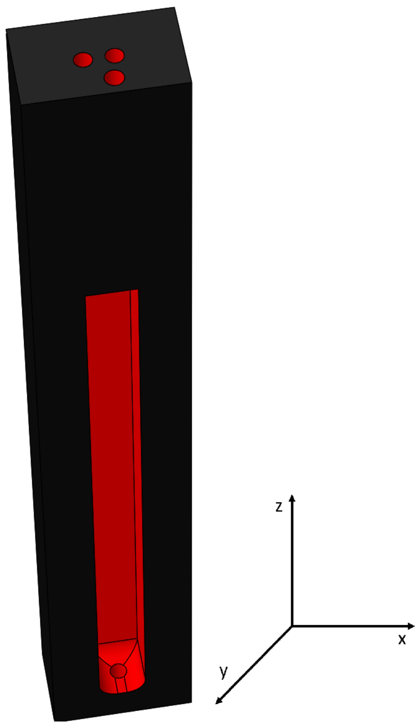

FIG. 3.1: An overview of the used 3D printed chip. The three inlets, main channel and the outlet can be seen.

To allow the particles to deflect without interacting with the channel wall, the channel dimensions should be big enough. Using the model as described in Sec.2.6, it can be calculated that the maximum expected deflection is around 2 mm in y direction. Based on this deflection, the channel size is chosen to be 5 by 5 mm. The height (z-axis) of the channel is chosen to be 7 cm so that the magnet position in height can be varied with. The further away from the particle inlet, the less the particle is influenced by effects from this inlet.

The chip design contains just one outlet, since the purpose of this chip design was to proof the presence of the Magnus effect only, not to further process the particles by sorting them. The outlet was placed there so that chip could be cleaned properly and such that some of the used particles could be retrieved.

To ensure particles to be clearly visible throughout the chip, the whole chip was

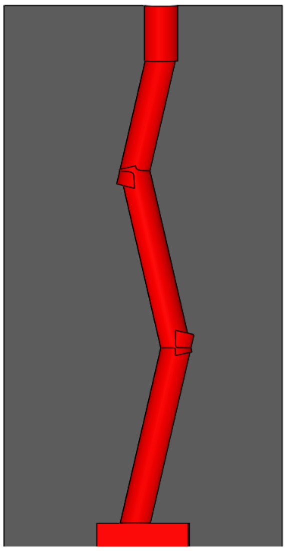

(A)

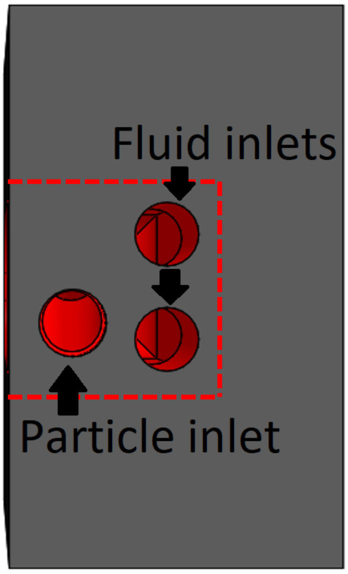

(B)

FIG. 3.2: An cross-section of the 3D chip to show the particle inlet, which is used for the focusing of the particles (A). The top view of the particle inlets at the top of the chip where the red dotted lines indicate the walls of the channel (B).

printed with a 3D printer with clear resin [18]. The smallest dimensions in this design, namely the diameter of the inlet and outlet of 800 μm, could be successfully printed. Nevertheless, the clear resin still made particles difficult to track. Therefore one side of the channel is left open and is covered with glass plate. This introduces some differences with the other 3 walls. However this should not have any influence on the behavior of the particle, because they should not interact with the walls at all.

3.2 Magnet choice

Two types of magnets are available, namely a permanent magnet and an electromagnet. The permanent magnet has some advantages over an electromagnet. The first advantage is that the permanent magnet's performance scales nicely with an increasing size. Therefore they produce a substantially higher bias field than an electromagnet for a certain volume of material. Furthermore there is no need for an external driving system for the magnet. For an electromagnet, the heating can be important, since this can change induced magnetic field [12]. A less important advantage is that a permanent magnet consumes no energy. To obtain a high torque, the field strength should be as high as possible. Furthermore, an low magnetic force is wanted and therefore the magnetic field should have a low gradient. This gives us the two main criteria for the magnetic field, namely a high field strength and low gradient. The field needs to be stable over time to prevent changes during the experiments. Based on these criteria a permanent magnet is chosen to create the external magnetic field.

Now that the type of magnet is known, several parameters can be chosen to optimize the system. The magnetic field should be as high as possible so that the applied torque is big. However the gradient of the field should be low across the channel for a low magnetic force. This implies that the field should be as homogeneous as possible throughout the channel. Therefore, the magnet dimensions should be much bigger in comparison to the channel dimensions. The magnet had dimensions of 50.8 x 50.8 x 25.4 mm. As a result of choosing a big magnet, the magnetic field will decrease slower over distance than a smaller magnet, resulting in a lower gradient.

3.3 Fluid selection

The type of fluid inside the channel through which the particles move is of importance for the particle's behavior. In general, two material properties can influence this behavior, namely the fluid density and viscosity.

The density of the liquid can influence the behavior of a particle in several manners. It determines how fast the particles sink or move upwards, because it influences the gravitational force as can be seen from Eq.2.23. Furthermore, it influences the deflection due to the Magnus force, as can be seen in Eq.2.20. If the density increases, the Magnus force increases. If the density of the liquid is chosen to be higher than the particles, the particles will flow up in the system. To create an inlet at the bottom of the chip would have as consequence that the fluid will flow out of the chip. Furthermore, high density liquids can be expensive. To avoid these problems, the density of the liquid was chosen to be lower than those of the particles. The particles have an average density of 2200 $\mathrm{kg\,m^{-3}}$, thus the density can be chosen between 500 of a low density liquid and 2200 $\mathrm{kg\,m^{-3}}$ of the particle.

The viscosity influences the system even more, because it influences the maximum rotational speed, all drag forces, the Magnus force and the magnetic force. In case of the liquid property viscosity, there is a trade off between the advantages of a high or low viscosity. A low viscocity results in a low drag force, which makes the particle move more easily through the liquid. However the sedimentation velocity of the particle also increases, which means that the particle is harder to track inside the system. The high viscosity liquid prevents the tracking problem, but also decreases the deflection due to the wanted Magnus effect. It also decreases the maximum rotation speed and in that way again the Magnus effect.

Taking into account all considerations, water and glycerol with a ratio of 3:1 is used. This liquid has a density similar to water of 1071 $\mathrm{kg\,m^{-3}}$ and a viscosity of 2.4 mPa s.

Chapter 4

Experimental

In this chapter the different materials and measurement setup and protocols will be discussed. First, the particles used during the research will be treated. Second, the equipment used in the setup will be mentioned. Third, the measurement set up for the VSM and Magnus effect experiment will be explained. Finally, the measurement protocols for the characterization of the magnet and the rotor will be treated. Furthermore, the measurement protocol for the Magnus effect will be explained.

4.1 Materials

4.1.1 FCC particles

FCC particles have been used with diameters varying between 40-150 µm and a density between 2700 and 3000 kg/m^3 [2]. During these experiments filtered particles with diameters between 70-90 µm have been used. Their magnetic moment is between 11.9 and 153 pAm^2 [1].

4.1.2 Janus particles

The particles used for the proof of principle were Janus particles, which can be seen in Fig.4.1. The black parts of the particles are the magnetic material. The yellow part of the particle is the non-magnetic material and is transparent. These particles are spheres made of borosilicate glass with a diameter between 70-90 µm and a density around 2200 $\mathrm{kg\,m^{-3}}$.The magnetic material is manganese iron oxide paramagnetic material (Fe_2MnO_4) and is applied on 30-50% of the particles' surface.

4.1.3 Equipment

During the research several things have been used for the performing of the experiments and analysis of the data.

The chip have been fabricated with a 3D printer from form labs, namely the Form 2 [18]. This printer is used with its clear resin form 2 FLGPCL02, it has a resolution of 25 µm and print structures of the size of 145 x 145 x 175 mm. The tensile strength of the material is around 65 MPa. This material does not solve or absorb most of the basic chemicals.

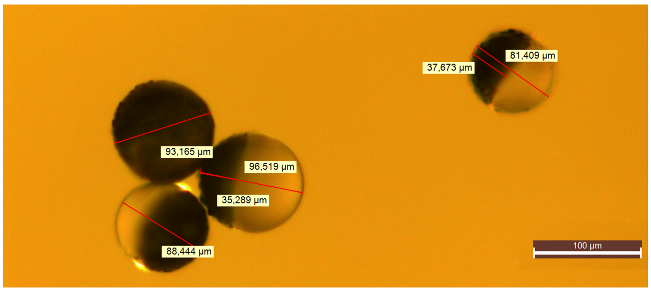

FIG. 4.1: An microscope image of the Janus particles. The black part of the particles is the layer of magnetic material. The yellow part is transparent glass with a yellow background.

The filling of the chip was done using the pumping device neMESYS from Cetoni with its user interface. The device consisted of a base module and three 290N modules [19]. The system is able to provide a wide spectrum of flow rates between 59.2 $\mathrm{nL\,min^{-1}}$ and 316 $\mathrm{mL\,min^{-1}}$.

The used liquid was a mixture of demineralized water and glycerol with a ratio of 3:1. Water has a density of 997 $\mathrm{kg/m^3}$ and a dynamic viscocity of 1 mPa s at 20 °C. At the same temperature, glycerol has a density of 1260 $\mathrm{kg/m^3}$ and a dynamic viscocity of 1413 mPa s.

The videos for the tracking of the particles were obtained using the Point Grey Grashopper 3 (GS3-U3-23S6m-C) is used together with its user software flycap2 [20]. The camera was operate at a frame rate of 100 FPS.

For the magnet, the so called Death magnet has been chosen [21]. This magnet has dimensions of 50.8 x 50.8 x 25.4 mm and has a weight of 500 gram. Furthermore, it has a magnetization in heigth (z-axis) of the magnet (25.4 mm) and a residual magnetism of 1.26-1.29 T.

For the characterization of the magnet the hall sensor SS94A1 is used [22]. This hall sensor can measure fields between -0.5 and 0.5 T. The accuracy of the system is determined by the multimeter to read its output voltage.

A rotor with a 3D printed mold will rotate the magnet during the experiments. The rotor is from Crouzet motors and has the serie number 82800802 [23]. If it is unloaded, it can go up to 24 V and a rpm of 4010.

To drive the rotor with a set voltage, the voltage supply Power supply ES 030-5 from Delta elektronika is used [24]. This supply delivers up to 30 V with a maximum current of 5 A.

For the characterization of the rotor and its rotation velocity, an heliostrobe will be used. In this case the HELIO-STROB micro2 is used [25]. This equipment can go from 1 rpm to 120.000 rpm.

The Quantum Design PPMS-VSM can measure the magnetic moment of the particles [26].

The simulations of the magnetic field is both done in Matlab [27] and Cades. Cades is a free software built to simulate magnetic fields and forces produced by permanent or electromagnets. The simulations of the trajectory of a particles was also done in Matlab. For the design of the 3D printed chip Solidworks has been used. The videos of the trajectories of the particles were analysed with ImageJ and a tracking script from Matlab [28]. The plots and analysis of the VSM data was done in GNUplot [29].

4.2 Measurement setup

4.2.1 VSM

To determine the magnetic properties of the Janus particles, 453 particles were placed between two 5x5 mm tape layers and placed inside the Quantum Design® PPMS-VSM. Subsequently, a magnetic field with varying strengths was applied, starting at 0T up to 5T after which a cycle was done from 5 to -5T and back to 5T again. This varying field is applied to characterize the particles. The change in magnetic field was 1.5 $\mathrm{mT\,s^{-1}}$. The temperature was set to 305 K.

4.2.2 Magnus effect

The top view of the total setup for the Magnus effect measurements can be seen in Fig.4.2. The chip is placed in the middle of the whole setup and is held in place by an external holder. This holder consists of a support with a gripper. The chip can be placed horizontally and vertically straight with a water level. The syringe pump will provide the liquid for the system with a tube connected to the chip, as can be seen in Fig.4.3. Pipette tips are placed inside the inlets and outlet to be able to connect the tubes. To prevent leakage, the connections have been glued to get a better sealing. The magnet together with the rotor will be placed in y-direction behind the chip in a holder. This holder consist of a non-magnetic support with a gripper. The distance between the chip and the magnet can be adjusted manually. There are two cameras placed at two sides of the chip. Camera 1 will follow the particles throughout the channel and record the movement in the x-direction, while the other camera will record the movement in the y-direction. This way the deflections in all directions are recorded. For a better contrast between the particle and the chip, the parts of the chip, where no camera is placed, are covered with black or white material for FCC and Janus particles respectively. This way the contrast between the background and the particles is increased. Another way to increase the tracking resolution was covering one side of the chip with glass glued on top of the chip.

4.3 Measurement protocol

4.3.1 Magnet placement

During the measurements different magnet placements will be used to characterize the magnetic force and Magnus effect. These different positions will be explained in

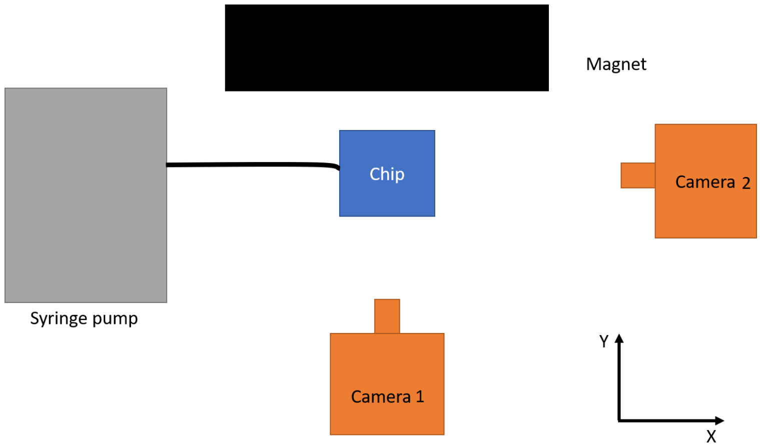

FIG. 4.2: The top view of the measurement setup used for the experiment of the Magnus effect. This figure is not on scale, but more a representation of the positing of the different equipment.

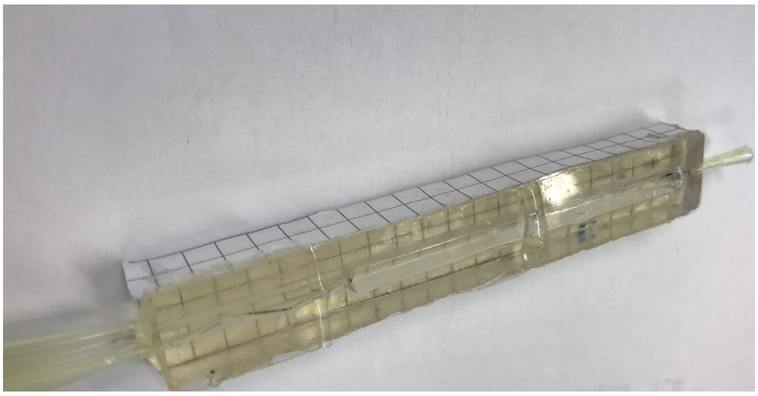

FIG. 4.3: A picture of the used chip during the experiments. At the left side of the picture the three pipette tips for the inlets can be seen. The side of the chip is covered with paper to get a better resolution for the tracking of the particles. The top of the channel is covered with glass to improve this resolution even more.

this section. To prevent the particle from getting attracted to the wall of the channel in the y-direction, the chip is placed at a distance D_y of 10 mm from the side of the chip, which is illustrated in Fig.4.4. This distance is similar for all experiments. The y-axis is defined to be 0 at the side of the chip covered with glass. The z-axis will be defined 0 at the middle of the magnet. This point is chosen due to the observation area during the measurements. The tracking of the particles will start at z=0 and will go down to z= -2 cm. So the (0,0,0)-point is inside the chip at the height of the middle of the chip in the middle of the channel. For the x-position of the magnet two different names for the scenarios will be used:

- Magnet middle: the magnet is aligned with the middle of the chip
- Magnet side: the middle of the magnet is shifted compared to the middle of the chip

The first scenario where the magnet placed in the middle of the chip can be seen in Fig.4.5. This scenario is used during the experiments to characterize the magnetic force and the Magnus force. The second scenario is that the magnet is placed with a predefined shift in the x-axis, which is illustrated in Fig.4.6. This is done to characterize the influence of the position of the magnet on the components of the magnet force and especially the x components. The x-component of the magnetic force is in the same direction as the Magnus effect. Therefore, it is crucial to determine the size of the magnetic force, so during the Magnus effect experiment this effect can be corrected for. The shift in the x-axis is defined as D_x and will be 10 mm. This scenario will be used during the characterization of the magnetic force only. However, the placement of the magnet during the experiments will not be perfect and therefore different D_y or D_x can occur. D_y and D_x are measured after the experiment and will be specified for each experiment.

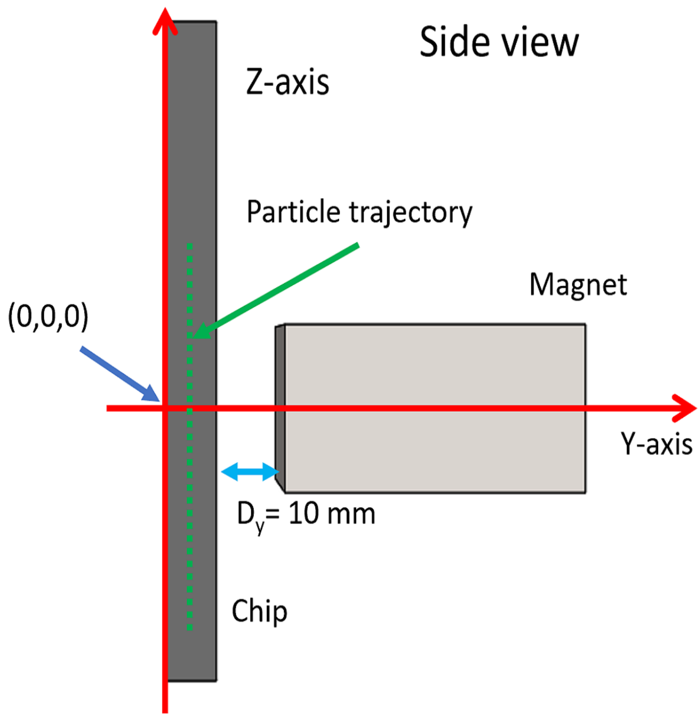

FIG. 4.4: The side view of the system indicating the positioning of the magnet compared to the chip. Furthermore the definition of the y- and z-axis can be seen. The distance between the chip and the magnet is defined with D_y.

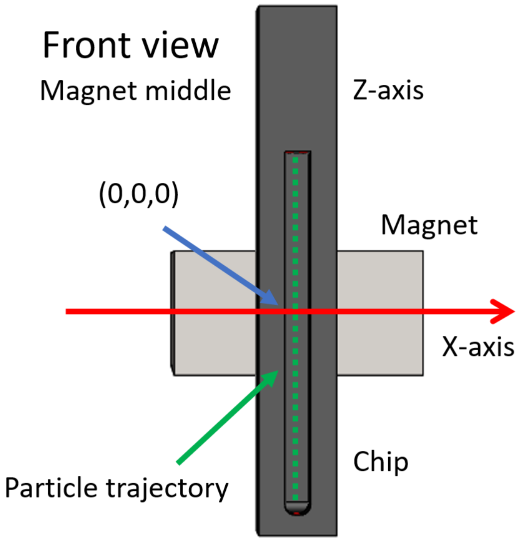

FIG. 4.5: The front view of the system indicating the positioning of the magnet compared to the chip. Furthermore the definition of the x- and z-axis can be seen. In this case the middle of the chip is aligned with the middle of the magnet and D_x is 0.

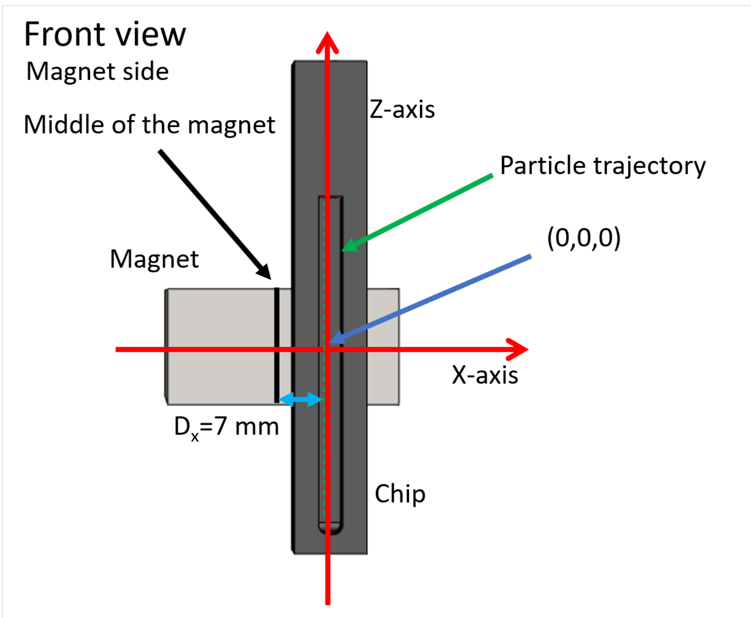

FIG. 4.6: The front view of the system indicating the positioning of the magnet compared to the chip. Furthermore the definition of the x- and z-axis can be seen. The distance between the chip and the middle of the magnet is defined with D_x and is 10 mm in this case.

4.3.2 Magnet characterization

To determine whether the magnetization of the magnet as stated by the supplier corresponds to the reality, a characterization will be conducted. The magnet will have the same orientation as in the setup of the Magnus effect experiment. The field strength will be measured at varying distances from the magnet by using a hall sensor.

4.3.3 Rotor characterization

For the rotor characterization the magnet and rotor will be placed with the same orientation as it will have during the Magnus experiments. A multimeter will measure the output voltage of the power supply, which powers the rotor. Subsequently, the rotational velocity of the rotor is determined for different voltages using an heliostrobe.

4.3.4 Magnus effect

The first step of the measurement is to position the chip properly by connecting the syringe to the chip and flow the liquid inside the chip. Then the chip is placed horizontally and vertically straight. This is done with the use of a water level. After the chip is placed properly, some particles are pipetted into the particle inlet.and tracked to determine if they fall straight. If needed, the chip can be tilted slightly if the particle path is not straight. This can be repeated until the particle path is straight. If this is the case the chip should not be moved or touched during the complete measurement. Then, similar tests are done to ensure the entire particle trajectory of both sides (front and side) in the channel is straight. When succeeded, the magnet can be placed inside the holder with the middle of the magnet and the middle of the channel outlined. The correct distance is determined by applying some particles inside the system and track the deflection in the y-direction. If the particles deflect too much and touch the wall, the magnet should be moved further away. If there is a big deflection in x-direction, the magnet is not placed properly in the middle and this should be adjusted. If everything is placed on the right position, the real experiment can be executed.

Each experiment has five different stages during which the trajectories of the particles will be recorded. Each stage is characterized by the magnet behavior:

1. No rotation
2. Rotation to the right
3. No rotation
4. Rotation to the left
5. No rotation

During the first stage, the magnet does not rotate. The magnet is placed horizontally with its magnetization along the height (z-axis) of the chip. This is done to observe the particle trajectory when they do not rotate. This stage will be used as reference for the next stage. During the next stage, the magnet will rotate with a certain rotation speed to the right. The rpm value is chosen priot to starting the experiment and the corresponding voltage will be applied using the power supply. The third stage is the same as the first stage as this stage is to check if the orientation of the chip hasn't changed during the experiment. The fourth stage is rotating the magnet to the left. The last stage is again to check the orientation of the chip.

4.4 Modeling

For the simulations of the magnetic field and forces both Matlab and Cades have been used. There are no boundary conditions set for the simulations in both programs. The only boundary given is the distance, area or volume where the field and forces need to be calculated. The precision of both programs is determined by the mesh of the calculations. The mesh size for Cades and Matlab are set to 10 steps per cm.

The model for the particle trajectory is created in Matlab. There are two limitations to the accuracy of the simulations, namely the mesh size and the time step size. The mesh size is set to the same size as the magnetic mesh size. The step size in time is set to be 0.002

Chapter 5

Results & Discussion

In this chapter the results obtained during this research will be shown. First, the VSM data to determine the magnetic properties of the particle will be presented. Second, the particle inlet will be discussed. Third, the modeled magnetic field strength will be validated with the use of a hall sensor. Fourth, the rotation length obtained during the experiments will be compared to the model, because this length determines how big the deflection due to the Magnus effect will be. Fifth, the x- and y-components of the magnetic force will be validated to get an impression of how much the positioning of the magnet will influence the trajectories of the particles during the Magnus effect experiment. The x-component of the magnetic force is acting in the same direction as the Magnus force and will therefore be of big importance. Finally, the Magnus effect will be shown for Janus and FCC particles for the situation with one and two magnets.

5.1 VSM

The result from the VSM data of the Janus particles can be seen in Fig.5.1. In this figure the magnetic moment of the particles for a field varying from -5 T up to 5 T and back is plotted. A steep rise or fall in the measured magnetic moment can be seen around 0 T. Around 0.3 T the field starts to saturate the particles and the magnetic moment becomes constant for an increasing field strength. From Fig.5.1 several magnetic properties of the particles can be derived. An overview of these properties is presented in Tab.5.1

TAB. 5.1: The data obtained from the VSM measurement, where N is the amount of particles, m_0 the magnetic moment, χ the susceptibility, M_{sp} the magnetization of the magnetic material and r_{pmag} the radius of the particle with an magnetic layer.

N	m_0[pA m^2]		χ[nA m^2 T^{-1}]		M_{sp}[kA m^{-1}]	r_{pmag}[µm]	
	Total	Average per particle	total	Average per particle	theory	supplier info	experimental
451	2848	63	123	0.27	2.4[30]	46-47	47.7

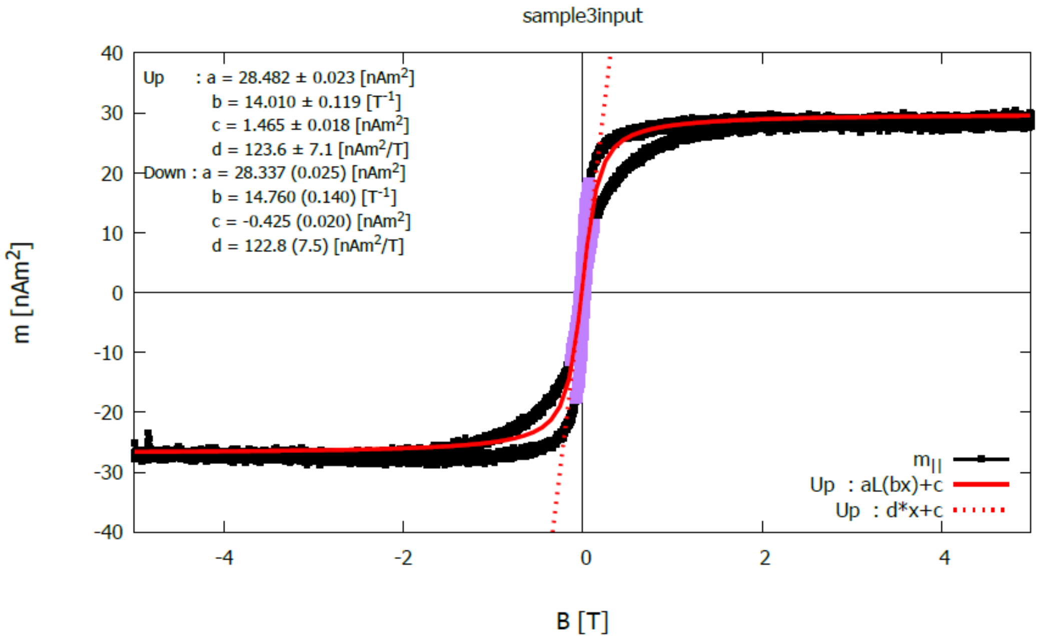

FIG. 5.1: The VSM data of the Janus particles with an applied magnetic field strength ranging from -5 T to 5T, where a is the saturation magnetization [m_0], b is the Langevin parameter [$\mu(K_B T)^{-1}$], c is the offset [nA m^2] and d the susecptibility [nA m^2 T^{-1}]

The magnetization (M_{sp}) of the magnetic compounds of the structure Fe_2O_4 was found in literature to be 2.4 kA m^{-1} [30]. Using this magnetization, the measured magnetic moment and Eq.2.19, the radius of the magnetic particle is calculated. The experimental determined radius is 47.7 µm, which is in agreement with the provided radius.

In order for the Janus particles to be suited as proof of principle for the FCC particles, they have to be similar to the FCC particles. The magnetic moment of both types of particles is in the same order and differ a factor of 1.5. This indicates that the Janus particles are a good representation of the FCC particles due to their similar size, density and magnetic moment. An interesting thing to notice is that the magnetic moment of some of the FCC particles is even higher than the Janus particles. The unwanted accumulation of the Fe to a FCC particle causes a higher magnetic moment than a Janus particle, which are designed to be super-paramagnetic.

5.2 Particle inlet

The starting position of a particle inside the channel is crucial for their trajectory. Therefore the starting position of different particles should vary as little as possible. A particle inlet, which will focus the particles, is designed based on the gravitational force. The functioning of the particle inlet can be seen in Fig.5.2. A particle moving through the three different cylinders is shown at different points in time. In Fig.5.2a the particle enters the inlet and sedimentates to the surface of the first cylinder in

Fig.5.2b. Afterwards, it will roll across the surface. These steps will repeat after the particle rolls out of the first cylinder into the second one, as is shown in Fig.5.2c and Fig.5.2d. When the particle rolls out of the third outlet, it will deflect towards the right in the x-direction, as can be seen in Fig.5.2g and Fig.5.2h. The velocity of the particles is similar and therefore an stable starting position is created. The difference in starting position was found to be 100 µm, which is a bit larger than the diameter of 1 particle.

The particle moves through the particle inlet as intended. It rolls over the surface of the channel with a similar velocity, which results in a starting position inside the channel that varied only 200 µm in the x-axis.

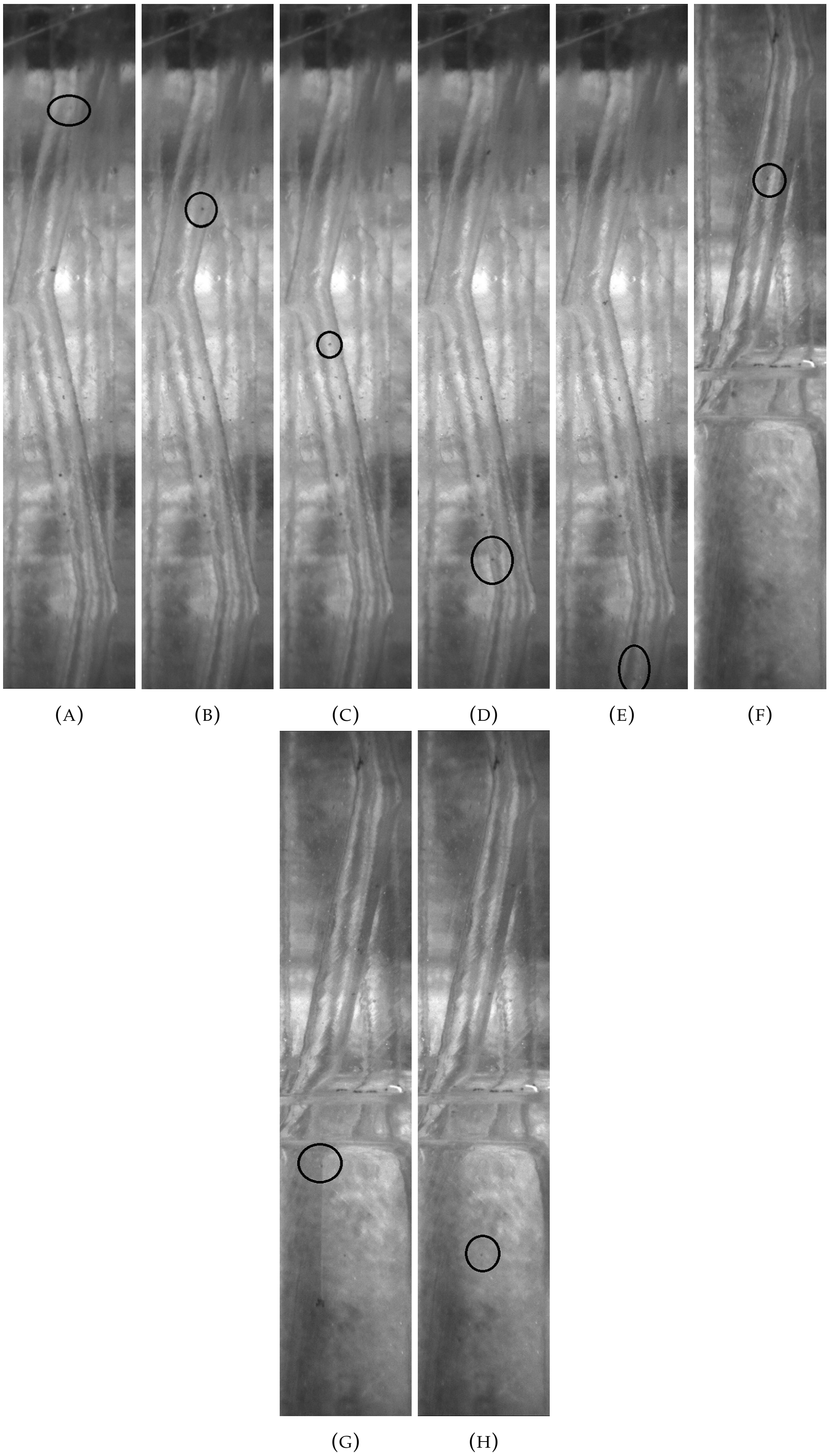

FIG. 5.2: A particle moving through the three cylinders of the particle inlet at different points in time. The particle moves due to gravity through the inlet and into the channel.

5.3 Magnetic field

5.3.1 Field strength

The calibration of the magnetic field strength of one and two magnets is shown in Fig.5.3 and Fig.5.4 respectively.

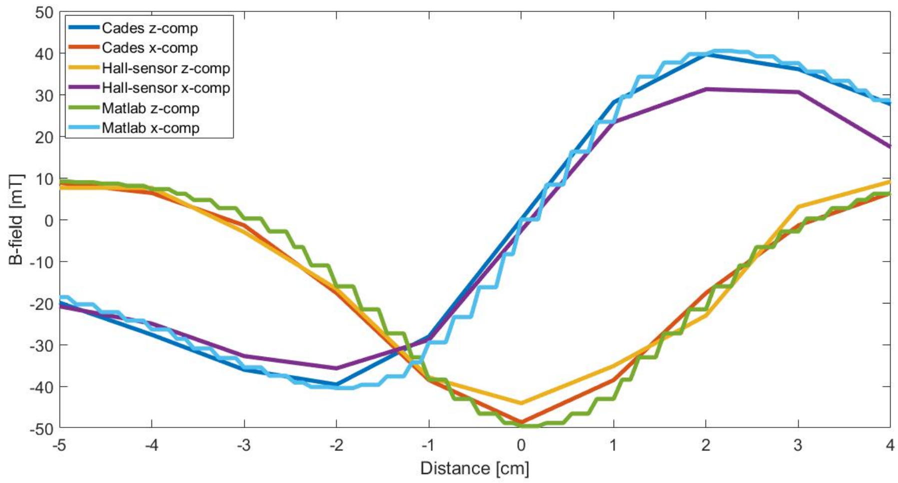

FIG. 5.3: The x- and z-component of the field strength over distance in the z-axis for one magnet measured with a hall sensor and modeled with Matlab and Cades. Both components are measured along the z-axis with a fixed offset of 3 cm in x-direction.

Fig.5.3 shows that the magnetic field components vary over distance. The measured behavior of the field is similar to the behavior in the simulations in Cades and Matlab. However, there are some points where the measured field differs from both models, which can be caused by several factors. The first is the orientation dependency of the hall sensor. The measuring area of the hall sensor needs to be 90° compared to the direction of the field. If this orientation differs a few degrees, the measured field strength can differ from the real value. Another reason is the inaccuracy in determining the position of the measurement. The field is position dependent and a difference between modeled distance and measuring distance can result in a difference between the two. However the measured field indicates that the models are sufficiently accurate.

The measured field strength of the two magnets is in agreement with the model in Matlab, execpt the z-component. For distances smaller than 3 cm the hall sensor reached the maximum field strength it is capable of measuring. The output of the hall sensor therefore clip and the measured field becomes stable. Only distances over 3 cm are being compared with the model for the z-component. The differences between measurement and model are in this case bigger compared to the situation with one magnet. This can be caused by the orientation and positioning of the hall sensor, but the misalignment between the two magnets can also cause these small differences. Between the two magnets, a little piece of plastic is stuck, which creates

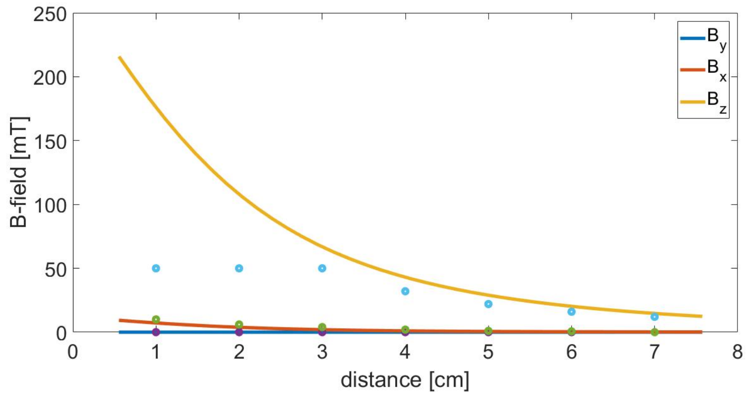

FIG. 5.4: The x- and z-component of the field strength over distance in the z-axis for two magnets measured with a hall sensor and modeled with Matlab and Cades. Both components are measured along the z-axis with a fixed offset of 3 cm in x-direction.

a misalignment of around 1 degree between the two magnets. The misalignment can have as consequence that the field is higher at some places and lower at others. However, the model is accurate enough to predict the created magnetic field created by one or two magnets.

5.3.2 Rotation length

To predict the rotation length of a particle through the channel, the field strength acting upon a particle is plotted versus the minimum needed field strength in Fig.5.5. The minimum field strength is obtained with Eq.2.39. This value is the minimum needed strength to overcome the rotational drag force and is obtained by using the properties of the particle, like the radius and magnetic susceptibility, and the properties of the fluid, like the viscosity. The field strength is plotted for a D_y of 10 mm and D_x of 0 mm. The particles start at the top of the channel, which is represented by z= 3 cm, and sedimentate to the bottom, which is represented by z= -4 cm.

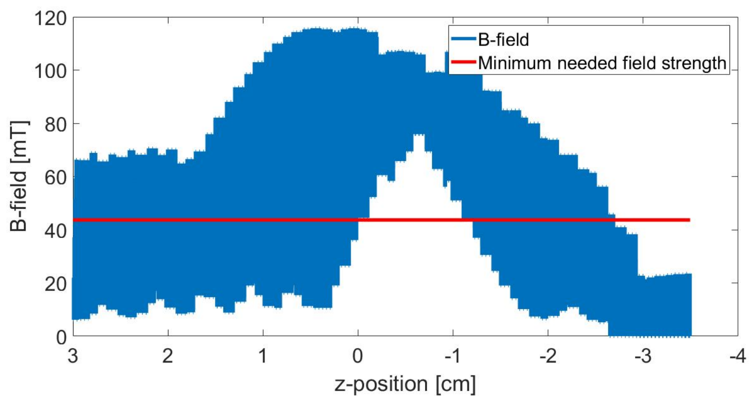

FIG. 5.5: The field strength is plotted over distance in the z-direction for one magnet for a D_y of 10 mm and D_x of 0 mm. The red line represents the minimum needed magnetic field to overcome the rotational drag for an rps of 5.

In this figure it can be found that there are three different region:

1. The field strength is lower than the minimum needed strength ($z < -3$)
2. The field strength is higher than the minimum needed strength ($-1 < z < 0$)
3. The field strength varies around the minimum needed strength ($z > 0$ & $-3 < z < -1$)

These three different regions will result in different particle behavior. In the first region, the field strength is too low to rotate the particle and the particle will move through the channel without rotating. During the second region, the particle will follow the magnetic field the complete rotation. The length of this region is used in this research as the distance of which the particle is properly rotating. An example of a proper particle rotation is shown in Fig.5.6. A simulated version of the last region is showed in Fig.5.7. The magnetic field is some parts of the rotation of the magnet higher than the needed strength and sometimes lower, which will result in a wobbling behavior of the particle. If the field strength is too low the particle will just move, but when the magnet rotates further the field can overcome the rotational drag. An example of a particle that cannot follow the magnetic field for a complete rotation is shown in Fig.5.8.

During the experiments the rotation length for both one magnet and two magnets is found to be slightly lower than the theoretical one for the Janus particles. For one magnet the model describes a rotation length of 10 mm, while an experimental length of 8 mm is found. The main advantage of using two magnets is the resulting rotation length of 30 mm, which is a factor 3 higher than the rotation length as a result of one magnet, as can be found in Fig.5.9. During the experiments a rotation length of 16 mm is found. The difference between the modeled and measured rotation length can be caused by some simplifications made in the model. First, the roughness of a particle is not taken into account, which will increase the rotational drag force. Second, the particle will not be perfectly round. The different shape will have a higher drag force coefficient, which increases the drag force. Finally, the placement of the magnet will never be in full agreement with the model. The orientation can be a few degrees off or the distance between a particle and the magnet can vary slightly between the model and the experiment. All together, these factors could explain the difference between the experimentally obtained and modeled rotation length. However, both rotation lengths have to same order of magnitude.

The same experiment have been performed for the FCC particles. These particles rotated for the whole observation length of the camera during their experiment for at least a distance of 20 mm in the y-direction. Assuming that the used model for the Janus particles is valid, it indicates that the used particles had a larger magnetic moment than expected. Miguel et al found that the sorted particles have a magnetic moment of 153 $\mathrm{pA\,m^2}$ [1]. This is slightly higher than the Janus particles used, but their rotating length shows that the FCC particles are better suited to rotate and have a higher moment than measured.

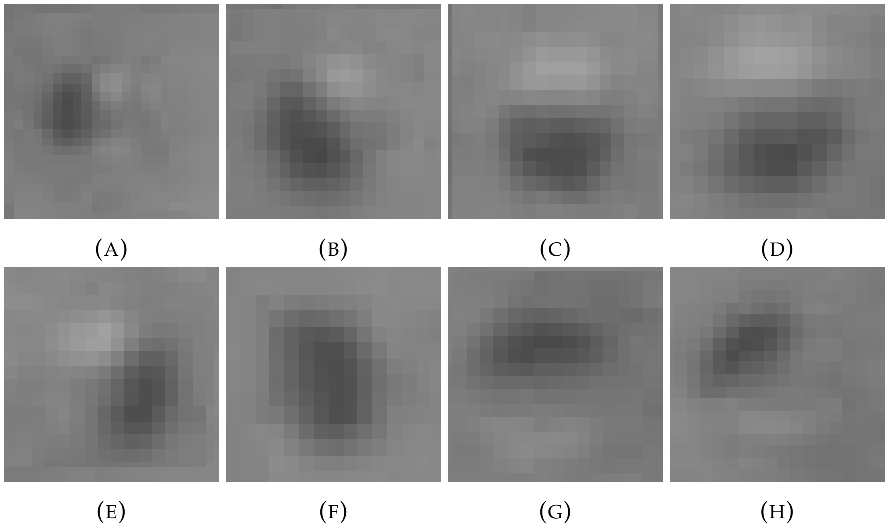

FIG. 5.6: A particle shown at different time points during a rotation. The particle can follow the complete rotation of the magnet, which is concluded from the black magnetic material rotating a complete round around the particle.

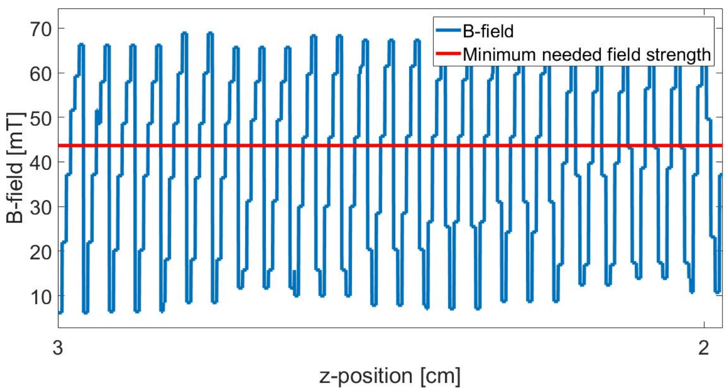

FIG. 5.7: The field strength is plotted over a short distance in the z-direction for one magnet for a D_y of 10 mm and D_x of 0 mm. The red line represents the required magnetic field to overcome the rotational drag.

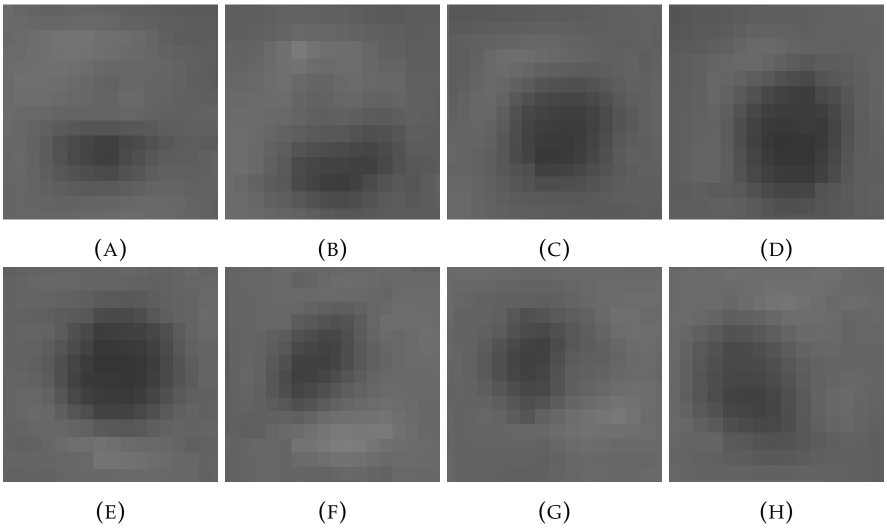

FIG. 5.8: A particle shown at different time points during a rotation. The particle cannot follow the complete rotation of the magnet and will move different compared to a proper particle rotating as can be seen in (D,E).

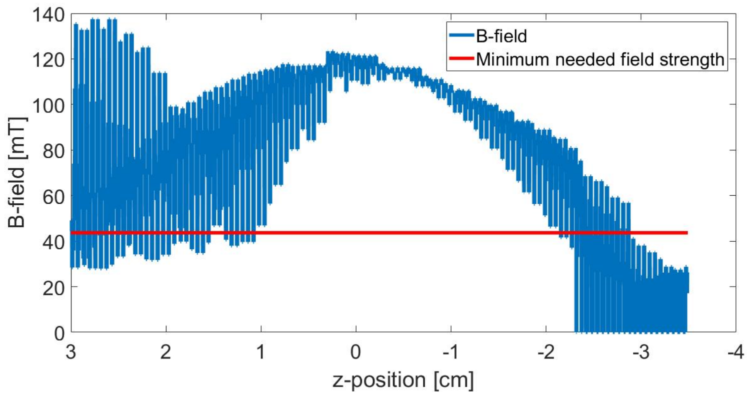

FIG. 5.9: The field strength is plotted over distance in the z-direction for two magnets for a D_y of 10 mm and D_x of 0 mm. The red line represents the required magnetic field to overcome the rotational drag for a rps of 5.

5.4 Magnetic force

5.4.1 Magnetic force in y-direction

The force created by the gradient of the magnetic field needs to be characterized. For the y-component of the force, this is done by first letting the particles sedimentate without an external magnetic field. Next, the magnet is placed at the two different magnet positions magnet middle and magnet side to observe the deflection due to the magnetic force. The resulting deflection for one magnet and two magnets can be seen in Fig.5.10 and Fig.5.11, respectively. In both cases 5 particles in each direction have been tracked and the resulting average deflection with their standard error are shown. During the magnet middle the position of the magnet was D_x=2 and D_y=10 mm and during the magnet side position, the magnet was placed at D_x=9 and D_y=10 mm. The trajectories of the particles without an external field are corrected so they fall straight down for both one and two magnets. From these results two different things can be noticed. First, the positioning of the magnet in x-direction barely influences the attraction of a particle in y-direction for both one and two magnets, which can be concluded from the same slope of both lines. The small difference in deflection in y-direction is caused by the positioning of the magnet in y-direction. Second, the modeled displacement of the particles correlates with the measured displacement in case of the two magnet experimental set up. However, for the case of one magnet a difference is observed. The modeled attraction decreases after 15000 µm in z-direction, where the measured attraction remains constant, which results in a bigger deflection.

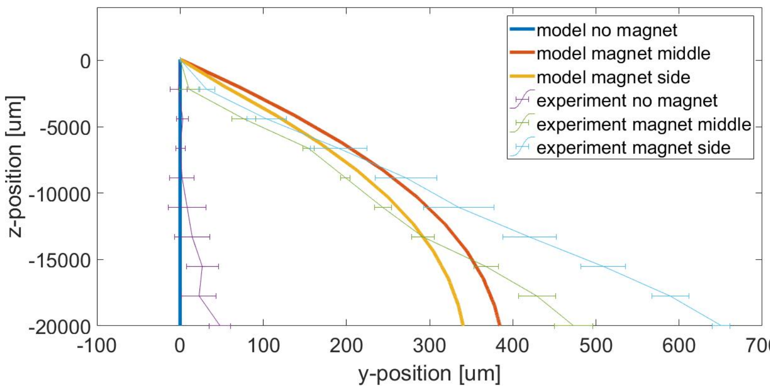

FIG. 5.10: The deflection of a particle towards one magnet in y-direction while it moves from the middle of the magnet to the lower edge of the magnet inside the chip.

5.4.2 Magnetic force in x-direction

For the characterization of the x-component of the magnetic force, the same positioning of magnet middle and magnet side was used. The characterization of the x-component is crucial, because it is acting in the same direction as the Magnus effect.

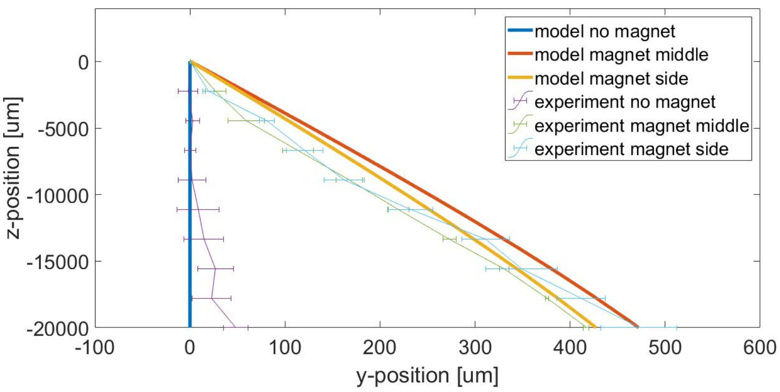

FIG. 5.11: The deflection of a particle towards two magnets in y-direction.

During the Magnus effect experiment, it is needed to compensate for the magnetic force. The experiment starts by first letting the particles sedimentate through the channel without a magnet. Next, the middle of the magnet is placed in the middle of the channel after which it is placed at the position of magnet side. The results for one magnet can be found in Fig.5.12. The difference in D_x is compensated for, so that each trajectory start all at 0,0,0. The trajectories of the modeled and measured one are similar, which can not be said for the slope. This difference can be caused by the grid size of the model. The starting position of the model can only be varied by one millimeter, which has a big influence on the obtained slope. For a starting position D_x of 3 mm in, the deflection is 82 µm, while it is 105 µm for a D_x of 4 mm. It is expected that the model becomes more accurate and will fit the data if the grid size is decreased.

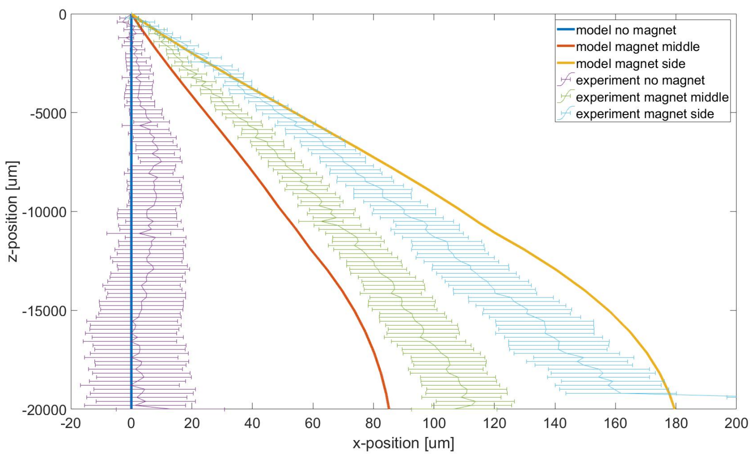

FIG. 5.12: The deflection of an particle in the x-direction for one magnet due to the x-component of the magnetic force for the three different situation. The first is no magnet. The second is magnet middle and lastly there is magnet side. Here is compensated for the difference in starting position in D_x compared to the magnet, so all trajectories start at 0.

The results of the experiment with two magnets can be found in Fig.5.13, where the different starting position in D_x is compensated for too. The main thing to notice about this result is the size of the standard error. The error bars are overlapping in a big part of the trajectories. The deviation of the individual particles is in the same range as the obtained deflection. The model predicts a slightly different deflection than measured. The reason is again the grid size of the model, because for a D_x of 1 or 1.5 mm, the model predicts a deflection of 0 or 15 µm, respectively. The shape of the trajectories of both the measured and modeled are in agreement, so the only difference is the deflection.

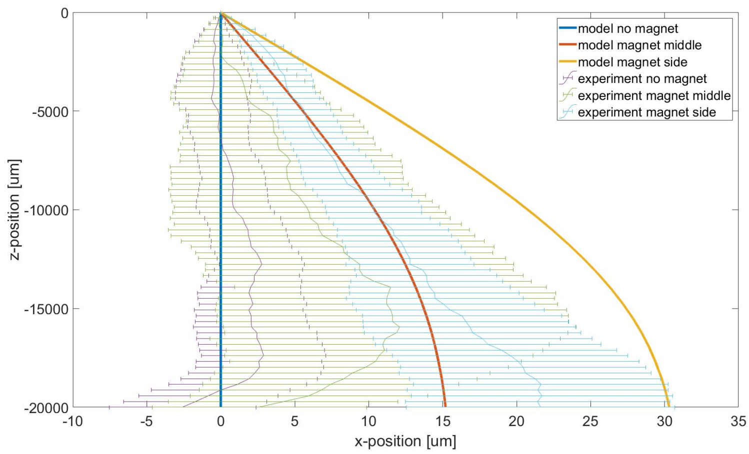

FIG. 5.13: The deflection of a particle in the x-direction for two magnets due the x-component of the magnetic force for the three different situations: 1) no magnet, 2) magnet middle and 3) magnet side. The difference in stating position in D_x compared to the magnet is compensated for, so all trajectories start at 0.

The model fits the deflection in x- and y-direction for one and two magnets. The differences in deflection are caused by the grid size of the model, but the shape and slope of the trajectories are in agreement.

5.5 Magnus effect

5.5.1 Janus

The validation of the model for the Magnus effect with Janus particles are done with both one and two magnets. The first, third and fifth stage of the experiment are called no Magnus (Sec.4.3.4). The counter clockwise and clockwise rotation, which will cause a deflection to the right and left, respectively, are called rotation right and left correspondingly. The magnet is placed at a D_x of 3 mm and a D_y of 8 mm. During each state of the experiment, 15 particles have been analyzed. The result of the experiment can be seen in Fig.5.14. The first thing to notice is the size of the standard error. This implies that the deviation between individual particles in all stages are in the same range as the displacement due to the Magnus effect. However, This result demonstrates a different behavior for no rotation of the magnet, a rotation right and a rotation left, which can be concluded from the average tracjectories of the different stages. The model predicts predicts a lower deflection due to the Magnus effect than found during the experiments. This conclusion can be drawn by the bigger difference between the rotating left and right compared to no Magnus of the measured than the modeled one. However, the deflection due to the Magnus effect is too small to overcome the deviation inside the system and therefore the Magnus effect is not yet proven.

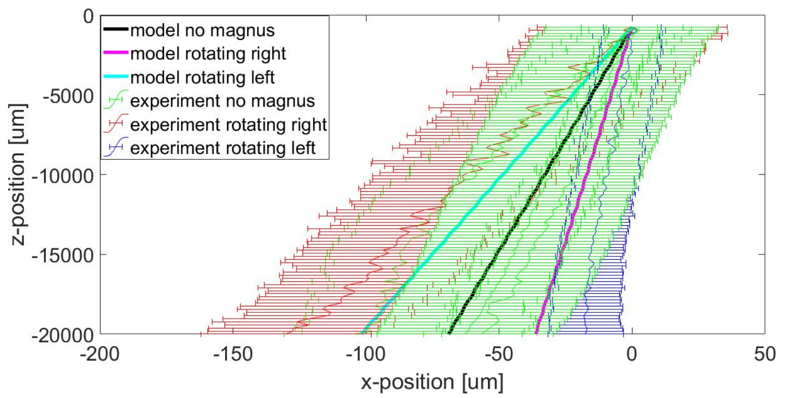

FIG. 5.14: The average trajectories with their standard error of the particles during the different stages of the experiment with one magnet. The displacement of the particles are in the same range as expected from the model, but their standard errors are overlapping during their whole trajectory.

The result of the experiment with two magnets shows a better distinction between the different stages, as can be seen in Fig.5.15. The standard error of the particles with no Magnus and deflecting to the right are not overlapping. However, the measured deflection is smaller compared to the modeled one, which can be caused by the difference in rotation length. If the deflection to the left is compared with no Magnus, the distinction is less obvious. Only close to -200000 in z-position, the standard error of both trajectories are not overlapping anymore. Here the deflection due to the Magnus effect is really similar to the model. This should not be the case due to the shorter rotation length of the particles during the experiments. The steepness of the slope of particles rotating left is steeper than modeled, which would indicate that the rotation velocity of the particles is higher than modeled.

For both one magnet and two magnet, the deflection in x-direction due to the magnetic force of the static magnet is predicted properly. However, the standard error of the results is big, which shows a big deviation in trajectory between particles. This deviation is bigger than expected based on previous experiments. The deviation can be caused by a change in magnet position or some unwanted flow inside the channel. Despite the big standard error on the no Magnus trajectory, the result is a good indication that a Magnus effect is happening inside the system. This conclusion is based on the difference in direction of deflection for a particle rotating right or left. Furthermore, the modeled deflection is in the same range as the measured one.

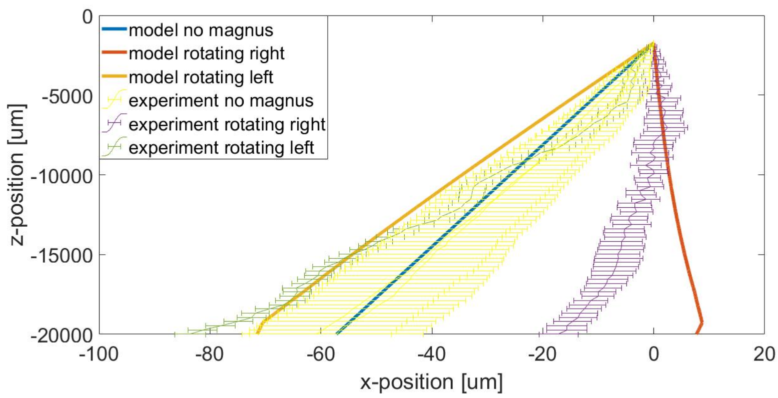

FIG. 5.15: The average trajectories with their standard error of the particles during the different stages of the experiment with two magnets. The displacement of the particles are in the same range as could be expected from the model and their standard error are only partly overlapping.

An interesting thing to look at is the size of the forces acting upon the particle in the x-direction, which are the Magnus force and the x-component of the magnetic force. The strength of the forces are plotted in Fig.5.16. The Magnus force is constant over the whole channel, while the magnetic force is position dependent. However, everywhere in the channel the Magnus force has a bigger strength compared to the magnetic force.

5.5.2 FCC

During the experiment for FCC particles, the placement of the magnet was different compared to the Janus particles. The magnet was placed at a D_x of 3 mm and a D_y of 20 mm, which is twice as far in y-direction as during the experiment with the Janus particles. This choice is made on the observation that FCC particles flowing through the channel have a larger deflection towards the magnet in the y-direction compared

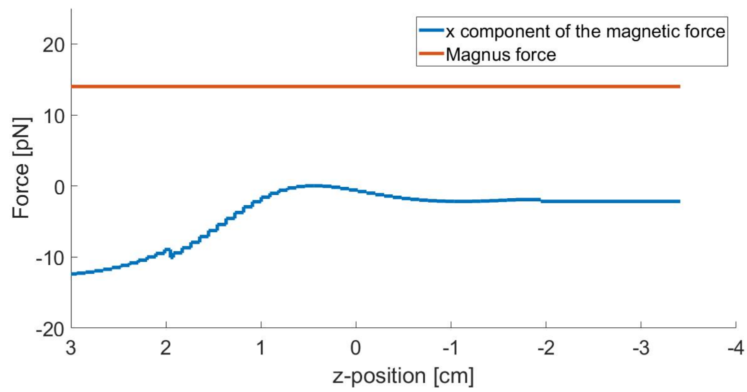

FIG. 5.16: The strength of the Magnus force and the x-component of the magnetic force over distance.

to the Janus particles. This supports the assumption that the magnetic moment of the FCC particle is bigger than the measured moment of the sorted particles [1]. Due to a scarce amount of sorted particles, only 5 particles were used for each state with no Magnus. For the rotating left and right, only 9 and 5 particles were used, respectively. For the FCC particles, the result is even better than the Janus particles, as can be seen in Fig.5.17. The standard error on the trajectories of the different signal are overlaping nowhere and can be distinguished properly. When the model for the Janus particles is taken as an expectation for the deflection due to the Magnus effect, the results of the FCC particles are in agreement with the model. The measured deflections are 37 and 45 µm for rotating left and right, while the model predicts a deflection of 25 and 64 µm for rotating left and right, respectively. This difference can be caused by the different magnetic moment of the FCC particle than the modeled magnetic moment for the Janus particles.

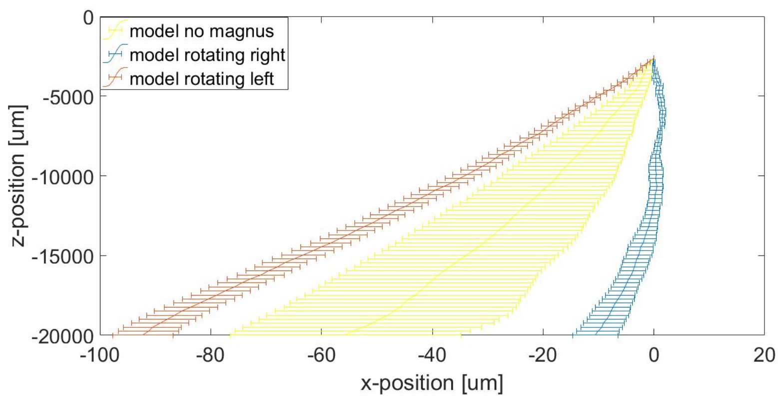

FIG. 5.17: The average trajectories of the FCC particles with their standard error of the particles during the different stages of the experiment with two magnets. The displacement of the particles are in the same range as the expected ones from the model and their standard error are not overlapping.

The difference in deflection of particles with and without Magnus effect is too small to sort the particles inside this 3D printed chip. To be able to achieve sorting of the particles using the Magnus effect inside a microfluidic chip, smaller dimensions between the outlets of the chip should be used. Also, the starting position of the particle inside the channel should be improved even more. Furthermore, the deflection due to the Magnus effect should be increased by changing the liquid or creating a higher magnetic field. This higher magnetic field will need to have a lower gradient to prevent the magnetic force to become dominant.

Chapter 6

Conclusions

During this research, it was investigated if the Magnus effect can be used to sort FCC particles inside a microfluidic chip. As the Magnus effect acts upon rotating particles, the FCC particles first need to be rotated. This is achieved by using an externally applied rotating magnetic field. This external field is created by using either one or two permanent magnets. The trajectory of a particle is simulated using a model made in Matlab. This model predicts several phenomena, such as the magnetic field, rotational length, gravitational force, magnetic force, torque and Magnus force in order to accurately describe the path of the particles. Due to the inhomogeneity between individual FCC particle properties like diameter, shape and magnetic moment, Janus particles were used to validate the model. The use of Janus particles for verification purposes is legitimate, since the particles have similar diameter and magnetic moment, which is measured using a VSM measurement. For the experiments, a microfluidic chip has been designed. This chip consists of a channel big enough for a particle to deflect due to the magnetic force and Magnus effect without interacting with the channel walls. Furthermore, a particle inlet is designed, which is able to focus the particle by using gravitational forces solely. The model for the magnetic field is validated using a hall sensor and a model in Cades. Although some small differences occur between the measured and modeled value, the model is sufficiently accurate to predict the magnetic field. The rotational length as found by the model turned out to be lower than the experimentally determined value for Janus particles. This is expected to be caused by the simplification made to determine the minimal magnetic field needed for a particle to overcome the rotational drag force. In contrast to the rotational length of the Janus particles, the rotational length of the FCC particles turned out to be longer than expected, which indicates that these particles have a higher magnetic moment than measured with a VSM measurement [1]. The model of the magnetic forces have been validated experimentally. A small difference in deflection distance was observed, which can be caused by the large grid size used in the model. It is shown that the y-component of the magnetic force barely depends on the position in x-direction. The experiment to sort the particles using the Magnus effect shows that the trajectories of the particles change depending on the rotation direction of the magnet. This dependency is in correspondence with the model based on Rubinov [17]. To be able to sort the particles, the particle starting position should be improved even more. To obtain a high performance sorter, the deflection due to the Magnus effect should be increased. This can be obtain by using a different liquid or increasing the magnetic field strength. If the magnetic force is decreased and the magnetic torque acting upon a particle inside the system is increased, the particles can potentially be sorted using the Magnus effect.

Bibliography

[1] M. Solsona et al. "Magnetophoretic Sorting of Single Catalyst Particles". In: *Angewandte Chemie* (2018). URL: https://onlinelibrary.wiley.com/doi/abs/10.1002/anie.201804942.

[2] F. Meirer et al. "Life and death of a single catalytic cracking particle". In: *Science Advances* 1.3 (2015).

[3] E. T. C. Vogt and B. M. Weckhuysen. "Fluid catalytic cracking: recent developments on the grand old lady of zeolite catalysis". In: *The Royal Society of Chemistry* 44 (May 2015), pp. 7342–7370.

[4] P. C. Rem, N. Fraunholcz, and E. A. Schokker. "MAGNUS SEPARATION". In: *Separation Science and Technology* 37.16 (2002), pp. 3647–3660. DOI: 10.1081/SS-120014824. eprint: https://doi.org/10.1081/SS-120014824. URL: https://doi.org/10.1081/SS-120014824.

[5] Jun Zhang et al. "Particle inertial focusing and its mechanism in a serpentine microchannel". In: *Microfluidics and Nanofluidics* 17.2 (2014), pp. 305–316. ISSN: 1613-4990. DOI: 10.1007/s10404-013-1306-6. URL: https://doi.org/10.1007/s10404-013-1306-6.

[6] O K Karaoglu R Rasooli. "Simulation of Particle Separation Using Inertial Microfluidics in a Spiral Microchannel for Biomedical Applications". In: (2016).

[7] G.K. Batchelor. *An introduction to fluid dynamics*. Cambridge University Press, 1967.

[8] Sir Horace Lamb. *Hydrodynamics*. Nature, 2004.

[9] Howard C Berg. *Random Walks in Biology*. Princeton University Press, 1993.

[10] Paul J. A. Kenis Daniel T. Chiu Wendy Zhang Howard A. Stone Rustem F. Ismagilov David Rosmarin and George M. Whitesides. "Pressure-Driven Laminar Flow in Tangential Microchannels: an Elastomeric Microfluidic Switch". In: (2001).

[11] E.P. Furlani. *Permanent Magnet and Electromechanical Devices; Materials, Analysis and Applications*. Academic, 2001.

[12] E.P. Furlani. "Analysis of particle transport in a magnetophoretic microsystem". In: *Journal of Applied Physics* (2006).

[13] Arijit Ghosh et al. "Analytical theory and stability analysis of an elongated nanoscale object under external torque". In: *Phys. Chem. Chem. Phys.* 15 (26 2013), pp. 10817–10823. DOI: 10.1039/C3CP50701G. URL: http://dx.doi.org/10.1039/C3CP50701G.

[14] Jeffrey Ryan Kensrud. "DETERMINING AERODYNAMIC PROPERTIES OF SPORTS BALLS IN SITU". PhD thesis. WASHINGTON STATE UNIVERSITY, 2010.

[15] *TeachPE*. URL: http://www.teachpe.com/biomechanics/fluid-mechanics/spin.

[16] L. G. Leal. *Advanced Transport Phenomena:Fluid Mechanics and Convective Transport Processes*. Cambridge University Press, 2007.

[17] S.I. Rubinov and J.B. Keller. "The transverse force on a spinning sphere moving in a viscous fluid". In: (1961).

[18] *Form 2 3D printer*. URL: https://formlabs.com/3d-printers/form-2/.

[19] *Cetoni*. URL: https://www.cetoni.de/en/products/low-pressure-syringe-pump-nemesys-290n/.

[20] *Point Grey*. URL: https://www.ptgrey.com/grasshopper3-23-mp-mono-usb3-vision-sony-pregius-imx174-camera.

[21] *Supermagnete*. URL: https://www.supermagnete.de/eng/block-magnets-neodymium/block-magnet-50.8mm-x-50.8mm-x-25.4mm-neodymium-n40-nickel-plated_Q-51-51-25-N.

[22] *Honeywell*. URL: http://www.farnell.com/datasheets/2012495.pdf?_ga=2.180200484.1848338336.1532004297-1760648949.1516789781&_gac=1.242339510.1532004297.EAIaIQobChMIOMi-2pir3AIVlB4bCh1AjgUVEAAYASAAEgI8gPD_BwE.

[23] *Crouzet Motors*. URL: https://nl.mouser.com/datasheet/2/92/dc-motors-dc-direct-drive-brushed-motors-42-mm-22--972909.pdf.

[24] *Delta Elektronika*. URL: http://www.delta-elektronika.nl/en/products/dc-power-supplies-150w-es150-series.html.

[25] *Elmed*. URL: https://www.elmedgmbh.com/en/products/stroboscopes-overview/helio-strob-micro2.html.

[26] *Quantum Design, VIBRATING SAMPLE MAGNETOMETER*. URL: https://www.qdusa.com/sitedocs/appNotes/vsmappnote_5-09.pdf.

[27] *Mathworks*. URL: https://nl.mathworks.com/products/matlab.html.

[28] *Motion-Based Multiple object Tracking in Matlab*. URL: https://nl.mathworks.com/help/vision/examples/motion-based-multiple-object-tracking.html.

[29] *GNU plot*. URL: http://www.gnuplot.info/.

[30] M. Venkatesan J. M. D. Coey and Hongjun Xu. *Introduction to Magnetic Oxides*. 2006.

Appendix A

Rolling chip

A.1 Rolling chip

Besides the idea to sort the particles based on their Fe distribution using the Magnus effect, another popped up. The deflection of a particles created by the Magnus effect is due to rotational friction of the particle with the surrounding liquid. In the new idea, the friction with the surroundings is increased by letting the particles roll over the bottom of the channel. Therefore, if the particle rotates, the particle will interact with the wall and will deflect. During experiments of the Magnus effect, some particles were close to wall and started to have a huge deflection in the x-direction. Based on this observation, the new idea is promising. This idea is already tried with two different versions of chips. The first version can be seen in Fig.A.1 and Fig.A.1. However, in this chip the particles were hard to track inside the chip due to the fact that the top of the channel was not parallel with the bottom of the channel. Therefore a second version has been designed and tested, which can be seen in Fig.A.3 and Fig.A.3. However, this chip didn't work due to the poor focusing of the particles. The poor focusing of the particles was due to some unwanted turbulance at the transition between the inlets and the channel. Due to limiting time, this idea couldn't be tested more. However, due to observations in the other experiments, it looks very promising.

FIG. A.1: The front view of first version of the chip where the particle roll across the bottom of the channel and deflect due to the friction with the wall when it is rotating.

FIG. A.2: The side view of first version of the chip where the particle roll across the bottom of the channel and deflect due to the friction with the wall when it is rotating.

FIG. A.3: The front view of second version of the chip where the particle roll across the bottom of the channel and deflect due to the friction with the wall when it is rotating.

FIG. A.4: The side view of first version of the chip where the particle roll across the bottom of the channel and deflect due to the friction with the wall when it is rotating.